Geochemistry Geophysics Geosystems G3
AN ELECTRONIC JOURNAL OF THE EARTH SCIENCES
Published by AGU and the Geochemical Society

Article
Volume 9, Number 4
1 April 2008
Q04003, doi:10.1029/2007GC001651
ISSN: 1525-2027

^{238}U-^{230}Th-^{226}Ra-^{210}Pb-^{210}Po, ^{232}Th-^{228}Ra, and ^{235}U-^{231}Pa constraints on the ages and petrogenesis of Vailulu'u and Malumalu Lavas, Samoa

Kenneth W. W. Sims and S. R. Hart
Department of Geology and Geophysics, Woods Hole Oceanographic Institution, Woods Hole, Massachusetts 02543, USA (ksims@whoi.edu)

M. K. Reagan
Department of Geoscience, University of Iowa, Iowa City, Iowa 52242, USA

J. Blusztajn
Department of Geology and Geophysics, Woods Hole Oceanographic Institution, Woods Hole, Massachusetts 02543, USA

H. Staudigel
Scripps Institution of Oceanography, La Jolla, California 92093, USA

R. A. Sohn
Department of Geology and Geophysics, Woods Hole Oceanographic Institution, Woods Hole, Massachusetts 02543, USA

G. D. Layne
Department of Geology and Geophysics, Woods Hole Oceanographic Institution, Woods Hole, Massachusetts 02543, USA

Now at INCO Innovation Centre, Memorial University, St. John's, Newfoundland and Labrador, Canada A1B 3X5

L. A. Ball
Department of Marine Chemistry and Geochemistry, Woods Hole Oceanographic Institution, Woods Hole, Massachusetts 02543, USA

Now at Advanced Mass Spectrometer Products, Scientific Instruments Division, Thermo Fisher Scientific Inc., 81 Wyman Street, Waltham, Massachusetts 02454, USA

J. Andrews
Department of Marine Chemistry and Geochemistry, Woods Hole Oceanographic Institution, Woods Hole, Massachusetts 02543, USA

Retired

[1] We report ^{238}U-^{230}Th-^{226}Ra-^{210}Pb-^{210}Po, ^{232}Th-^{228}Ra and ^{235}U-^{231}Pa measurements for a suite of 14 geologically and geochemically well-characterized basaltic samples from the Samoan volcanoes Vailulu'u, Malumalu, and Savai'i. Maximum eruption ages based on the presence of parent-daughter disequilibria indicate that Vailulu'u is magmatically productive with young lavas (<8 Ka) resurfacing both its summit crater and lower flanks. ^{210}Pb and ^{210}Po measurements indicate that several flows have erupted within its summit crater in the past 100 years, with the newest observed flow being erupted in November of 2004. For lavas which have eruption ages that are demonstrably young, relative to the half-lives of ^{230}Th,

^{231}Pa, and ^{226}Ra, we interpret their ^{238}U -^{230}Th, ^{235}U-^{231}Pa and ^{230}Th - ^{226}Ra disequilibria in terms of the magmatic processes occurring beneath the Samoan Islands. (^{230}Th/^{238}U) > 1 indicates that garnet is required as a residual phase in the magma sources for all these lavas. The large range of (^{238}U/^{232}Th) and (^{230}Th/^{232}Th) is attributed to long-term source variation. The Samoan basalts are all alkaline basalts and show significant ^{230}Th and ^{231}Pa excesses but limited variability, indicating that they have been derived by small but similar extents of melting. Their (^{230}Th/^{238}U), (^{231}Pa/^{235}U) and Sm/Nd fractionation are consistent with correlations among other ocean island basalt suites (particularly Hawaii) which show that (^{230}Th/^{238}U) and (^{231}Pa/^{235}U) of many OIBS can be explained by simple time-independent models. Interpretation of the ^{226}Ra data requires time-dependent melting models. Both chromatographic porous flow and dynamic melting of a garnet peridotite source can adequately explain the combined U-Th-Ra and U-Pa data for these Samoan basalts. Several young samples from the Vailulu'u summit crater also exhibit significant ^{210}Pb deficits that reflect either shallow magmatic processes or continuous magma degassing. In both cases, decadal residence times are inferred from these ^{210}Pb deficits. The young coeval volcanism on Malumalu and Vailulu'u suggests the Samoa hot spot is currently migrating to the northeast due to dynamic interaction with the Tonga slab.

Components: 18,698 words, 13 figures, 5 tables.

Keywords: U-series disequilibria; Samoa; eruption ages.

Index Terms: 1040 Geochemistry: Radiogenic isotope geochemistry; 1105 Geochronology: Quaternary geochronology; 1037 Geochemistry: Magma genesis and partial melting (3619).

Received 4 February 2007; **Revised** 25 November 2007; **Accepted** 24 December 2007; **Published** 1 April 2008.

Sims, K. W. W., S. R. Hart, M. K. Reagan, J. Blusztajn, H. Staudigel, R. A. Sohn, G. D. Layne, L. A. Ball, and J. Andrews (2008), ^{238}U-^{230}Th-^{226}Ra-^{210}Pb-^{210}Po, ^{232}Th-^{228}Ra, and ^{235}U-^{231}Pa constraints on the ages and petrogenesis of Vailulu'u and Malumalu Lavas, Samoa, *Geochem. Geophys. Geosyst.*, *9*, Q04003, doi:10.1029/2007GC001651.

1. Introduction

[2] It has been shown that the Samoan Islands and seamounts form a hot spot track with a systematic age progression of shield-stage volcanism, heading west from the hypothesized present-day hot spot location of Vailulu'u [*Hart et al.*, 2000, 2004]. In this scenario, the submarine volcano Vailulu'u is the leading edge of volcanism related to a mantle plume and is thus presumed to be the youngest. Malumalu seamount is at the eastern end of an older subjacent volcanic lineament. While there are numerous lines of observational evidence that indicate Vailulu'u is young, the actual eruption ages of its surface lavas are unknown (as are those from Malumalu).

[3] Time is an essential aspect of understanding geological processes. Without age constraints, many central questions about the evolution of the Samoan hot spot track and magma production rates can never be fully answered. To determine the ages of these young submarine lavas, we measured ^{238}U-^{230}Th-^{226}Ra-^{210}Pb-^{210}Po, ^{232}Th-^{228}Ra and ^{235}U-^{231}Pa for numerous lavas from the seamounts Vailulu'u and Malumalu. These U-and Th- daughter nuclides have half-lives ranging from 138 days up to 75 ka and enable us to establish age limits for eruption of these lavas. We have also determined a ^{210}Po ingrowth age for a sample from the historic volcanic cone, 'Nafanua', that was recently documented inside the summit crater of Vailulu'u [*Staudigel et al.*, 2006].

[4] Because many of these samples' eruption ages are definitively young relative to the half-lives of ^{230}Th, ^{231}Pa, and ^{226}Ra, we also interpret their ^{238}U-^{230}Th, ^{235}U-^{231}Pa and ^{230}Th-^{226}Ra disequilibria in terms of the magmatic processes occurring beneath the Samoan Islands. The dominant mode of melt production in intraplate oceanic volcanism, like the Samoan Islands, is adiabatic decompression of solid upwelling mantle material, and numerous studies have shown that measurements of ^{230}Th/^{238}U, ^{226}Ra/^{230}Th and ^{231}Pa/^{235}U in young basaltic lavas can provide fundamental information on melting rate (related to solid mantle upwelling rate), melt migration velocity, and extent of melting [*Sims et al.*, 1995, 1999; *Elliott*, 1997; *Bourdon et al.*, 1998; *Bourdon and Sims*, 2003; *Lundstrom et al.*, 2003; *Pietruszka et al.*, 2001].

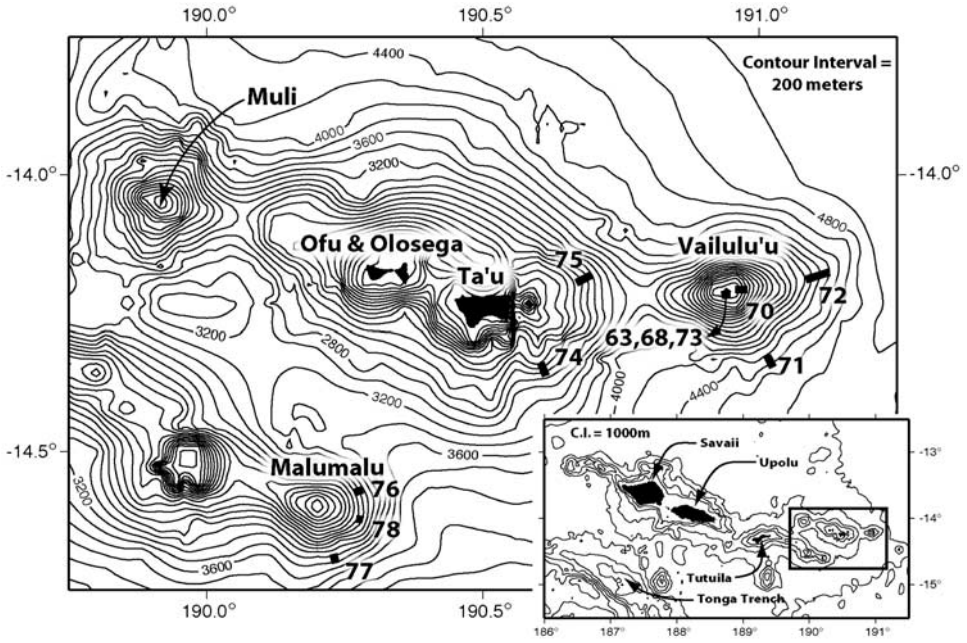

Figure 1. Map of the Samoan Islands (inset) and the AVON2/3 dredge locations on Vailulu'u and Malumalu for the samples analyzed in this study. Note the en echelon alignment of volcanic lineaments approximately along the N63W direction of Pacific plate motion. The distance from Malumalu to Ofu is 66 km, and from Malumalu to Vailuluu is 90 km.

[5] Finally, for samples with (^{210}Pb/^{226}Ra) < 1, we evaluate the potential for ^{210}Pb-^{226}Ra to provide information on magma degassing and recharge rates [e.g., *Gauthier and Condomines*, 1999; *Berlo et al.*, 2006; *Reagan et al.*, 2006; *Sims and Gauthier*, 2007].

2. Background

[6] The Samoan Islands and seamounts are located on the Pacific Plate between 12–15°S and 169–178°W (Figure 1) [*Hart et al.*, 2004]. The Samoan volcanoes are located along four en echelon volcanic lineaments [*Hart et al.*, 2004], subparallel to the direction of plate motion (N 63.4°W at 71 mm/yr). The western trend includes Savai'i, Upolu, and western Tutuila. The more easterly trends include eastern Tutuila to Malumalu, and Muli, Ofu/Olosega and Ta'u. Vailulu'u appears to be the beginning of a new trend. There is good evidence that these lineaments are an age-progressive hot spot track [*Hart et al.*, 2004].

[7] Vailulu'u is interpreted to be at the leading edge of the Samoan plume and is thus presumed to be the youngest. Recent volcanic activity at Vailulu'u has been documented by the newly mapped 300 m summit cone erupted between 1999 and 2005, and other supporting observations such as elevated water temperatures and high He, Mn and particulate contents within the summit crater [*Hart et al.*, 2000; *Staudigel et al.*, 2004, 2006]. Recent post-erosional stage volcanism is also observed on the islands of Tutuila, Upolu and the westernmost island of Savai'i, with the most recent eruptive episode taking place on Savai'i from 1905–1911.

[8] The samples analyzed in this study are shield-stage alkali basalts from the seamounts Vailulu'u and Malumalu, collected by dredging during the March 1999 AVON2/3 cruise of the R/V Melville [*Hart et al.*, 2000] and during the April 2005 ALIA cruise of the R/V Kilo Moana. These samples are a subset of the suite discussed in *Workman et al.* [2004] and *Sims and Hart* [2006]. We also included a posterosional-stage sample from the 1905 flow on Savaii [*Hauri and Hart*, 1993]. Sample descriptions and dredge locations are given in Table 1.

[9] Whole rock major-element compositions indicate that these samples are silica under-saturated alkaline basalts and trachybasalts that lie above the alkali-tholeiite line of *Macdonald and Katsura* [1964]. SiO_2 ranges from 44 to 49 wt% and MgO ranges from 5.8 to 27.4 wt%. The three samples with high MgO and lower SiO_2 abundances are picritic basalts with high modal olivine. Bulk silicate earth (BSE) normalized trace-element abun-

Table 1. Dredge Dates, Locations, and Depths[a]

Dredge	Name	Date	Location	On/Off Bottom	Latitude Degrees	Minutes	Longitude Degrees	Minutes	Depth, m	Median Depth, m	Length Dredge Track, m
ALIA - 101	VAILULU'U	7-Apr-01	Nafanua cone	ON	14	12.846	169	3.642	753	828	431
				OFF	14	12.848	169	3.402	904		
AVON 2/3 - 63	VAILULU'U	7-Mar-95	Crater floor	ON	14	13.06	169	3.91	712	920	1268
				OFF	14	13.05	169	3.12	894		
AVON 2/3-68	VAILULU'U	11-Mar-95	W crater wall	ON	14	13.00	169	3.60	975	780	887
				OFF	14	13.08	169	4.09	590		
AVON 2/3-70	VAILULU'U	12-Mar-95	E slope - summit cone	ON	14	12.50	169	1.28	1535	1130	2294
				OFF	14	12.50	169	2.55	725		
AVON 2/3-71	VAILULU'U	12-Mar-95	SE rift	ON	14	20.83	168	58.47	4421	4170	2687
				OFF	14	19.60	168	59.13	3919		
AVON 2/3-72	VAILULU'U	12-Mar-95	E rift	ON	14	10.60	168	52.36	4200	3835	4828
				OFF	14	11.42	168	54.92	3470		
AVON 2/3-73	VAILULU'U	13-Mar-95	Crater floor	ON	14	13.00	169	3.27	996	960	1120
				OFF	14	12.62	169	3.82	735		
AVON 2/3-76	MALUMALU	14-Mar-95	NE rift	ON	14	31.14	169	43.09	2785	2393	6366
				OFF	14	34.46	169	44.01	2005		
AVON 2/3-77	MALUMALU	14-Mar-95	SE rift	ON	14	42.08	169	46.01	3605	3237	1839
				OFF	14	41.11	169	46.24	2869		
AVON 2/3-78	MALUMALU	15-Mar-95	E rift	ON	14	37.35	169	43.57	2264	2225	314
				OFF	14	37.30	169	43.74	2187		

[a] Notes: (1) ALIA cruise on the R/V *Kilo Moana* and (2) AVON2/3 cruise on the R/V *Melville*.

Table 2. $^{230}Th/^{232}Th$, $^{234}U/^{238}U$ and U, Th, ^{226}Ra and ^{231}Pa Concentrations Measured by Mass Spectrometry[a]

Sample	[Th], ug/g	[U], ug/g	Th/U	($^{238}U/^{232}Th$)	($^{230}Th/^{238}U$)	($^{230}Th/^{232}Th$)	($^{234}U/^{238}U$)	^{231}Pa fg/g	($^{231}Pa/^{235}U$)	^{226}Ra, fg/g	($^{226}Ra/^{230}Th$)
Alia 101 (B1)	3.240	0.739	4.384	0.692	1.073	0.743	1.002			312	1.16
63-13 (A1)	4.992	1.135	4.399	0.690	1.069	0.738	1.003				
63-13 (A2)					1.068	0.737	1.003				
63-13 (B1)	4.998	1.133	4.413	0.688	1.070	0.736	1.001			*459*	*1.12*
63-13 (avg)	*4.995*	*1.134*	*4.406*	*0.689*	*1.070*	*0.737*	*1.002*				*1.12*
63-13(Pa)		1.150						496	1.33		
68-30 (A1)	3.523	0.818	4.306	0.705	1.086	0.765	1.004				
68-30 (B1)	3.498	0.809	4.323	0.702	*1.084*	0.761	1.001			346	1.17
68-30 (avg)	*3.511*	*0.814*	*4.315*	*0.703*	1.085	0.763	*1.002*				*1.16*
70-1 (A1)	3.957	1.000	3.956	0.767	1.013	0.777	1.007				
70-1 (B1)	3.978	0.996	3.995	0.759	1.026	0.779	1.002			399	1.16
70-1 (avg)	*3.967*	*0.998*	*3.976*	*0.763*	*1.019*	*0.778*	*1.004*				*1.16*
70-1 (Pa)		0.999						341	1.05		
70-9 (A1)	4.203	0.993	4.233	0.717	1.059	0.759	1.005				
70-9 (A2)					1.071	0.768					
70-9 (B1)	4.194	1.004	4.180	0.726	1.032	0.749	1.002			413	1.18
70-9 (avg)	*4.199*	*0.998*	*4.207*	*0.721*	*1.051*	*0.759*	*1.004*				*1.16*
70-9 (Pa)		0.997						361	1.11		
71-2 (A1)	2.296	0.535	4.289	0.707	1.045	0.739	1.005				
71-2 (B1)	2.273	0.528	4.310	0.704	1.033	0.727	1.001			214	1.16
71-2 (avg)	*2.285*	*0.531*	*4.299*	*0.706*	*1.039*	*0.733*	*1.003*				*1.15*
72-2 (A1)	5.151	1.213	4.248	0.714	1.065	0.761	1.001				
72-2 (A2)					1.059	0.756	1.003				
72-2 (B1)	5.220	1.222	4.272	0.710	1.062	0.754	1.001			428	0.98
72-2 (avg)	*5.186*	*1.217*	*4.260*	*0.712*	*1.063*	*0.757*	*1.002*				*0.98*
73-1 (A1)	5.997	1.242	4.830	0.628	1.089	0.684	1.004				
73-1 (B1)	5.962	1.248	4.777	0.635	1.056	0.671	1.002			469	1.05
73-1 (avg)	*5.980*	*1.245*	*4.803*	*0.632*	*1.072*	*0.677*	*1.003*				*1.04*
73-3 (A1)	4.834	1.073	4.504	0.674	1.100	0.741	1.003				
73-3 (B1)	4.840	1.067	4.534	0.669	1.089	0.729	1.001			447	1.14
73-3 (avg)	*4.837*	*1.070*	*4.519*	*0.671*	*1.095*	*0.735*	*1.002*				*1.13*
73-12 (A1)	5.074	0.984	5.159	0.588	1.144	0.672	1.005				
73-12 (A2)					1.151	0.677					
73-12 (B1)	5.110	0.979	5.220	0.581	1.161	0.675	1.001			384	1.00
73-12 (avg)	*5.092*	*0.981*	*5.190*	*0.585*	*1.154*	*0.675*	*1.003*				*1.00*
76-1 (B1)	6.367	1.216	5.238	0.579	1.055	0.611	1.003				
76-1 (Pa)		1.207						435	1.11		
77-9 (B1)	6.681	1.296	5.155	0.589	1.103	0.649	1.004				
78-1 (A1)	5.753	1.101	5.224	0.581	1.050	0.610	1.004				
78-1 (B1)	5.832	1.115	5.233	0.580	1.024	0.594	1.003				
78-1 (B2)					1.023	0.593				407	1.06
78-1 (avg)	*5.793*	*1.108*	*5.228*	*0.580*	*1.032*	*0.599*	*1.003*				*1.05*
SAV B6 (A1)	3.341	0.743	4.496	0.675	1.126	0.760	1.002				
SAV B6 (B1)	3.381	0.750	4.509	0.673	1.138	0.766	1.002			308	1.07
SAV B6 (avg)	*3.361*	*0.746*	*4.503*	*0.674*	*1.132*	*0.763*	*1.002*				*1.08*
					Quality Assurance						
ATHO	7.398	2.246	3.294	0.921	1.099	1.012	1.002			825	0.990
ATHO	7.574	2.277	3.326	0.912	1.111	1.013	1.001			861	1.009
ATHO	7.456	2.234	3.338	0.909	1.111	1.010	1.002			845	1.009
TML	29.516	10.525	2.804	1.082	1.001	1.083	1.000			3557	1.000
TML	30.580	10.640	2.874	1.056	1.008	1.064	1.003			3580	0.989
TML	29.822	10.521	2.835	1.070	0.991	1.061	1.002			3454	0.981
TML	31.820	11.201	2.841	1.068	0.994	1.062	1.002			3678	0.978
TML										3750	0.997
KL-31-KWWS-92		0.292						103	1.08		
HK-04-KWWS-92		0.665						389	1.80		

Table 3. ^{214}Pb, ^{214}Bi, ^{228}Ac, and ^{208}Tl Activities Measured by Gamma Spectroscopy[a]

Sample	(^{226}Ra), dpm/g	(^{214}Pb), dpm/g	1σ Rel Std	(^{214}Pb/^{226}Ra)	(^{214}Bi), dpm/g	1σ Rel Std	(^{214}Bi/^{226}Ra)	(^{232}Th), dpm	(^{228}Ac), dpm/g	1σ Rel Std	(^{228}Ac/^{232}Th)	(^{208}Tl), dpm/g	1σ Rel Std	(^{208}Tl ^{232}Th)
Alia 101-01	0.68	0.67	5%	0.99	0.66	6%	0.96	0.79	0.85	7%	1.08	0.87	7%	1.10
63-13	1.01	0.99	3%	0.98	0.93	4%	0.92	1.22	1.31	5%	1.07	1.19	5%	0.98
68-30	0.76	0.71	4%	0.93	0.84	6%	1.11	0.86	0.87	7%	1.02	0.98	7%	1.14
70-1	0.88	0.84	3%	0.95	0.78	6%	0.90	0.97	1.04	7%	1.07	0.96	7%	0.99
70-9	0.91	0.88	3%	0.97	0.84	5%	0.92	1.03	0.94	7%	0.92	1.07	7%	1.04
71-2	0.47	0.45	5%	0.97				0.56	0.58	9%	1.03			
72-2	0.94	0.96	2%	1.02	0.94	4%	1.00	1.27	1.26	5%	1.00	1.26	5%	0.99
73-1	1.03	0.99	4%	0.96				1.46	1.45	7%	0.99			
73-3	0.98	0.98	2%	1.00	0.97	4%	0.99	1.18	1.24	4%	1.05	1.18	4%	1.00
73-12	0.84	0.82	3%	0.98	0.85	6%	1.02	1.24	1.14	8%	0.92	1.22	8%	0.98
76-1														
77-9														
78-1	0.89	0.88	3%	0.99	0.90	5%	1.01	1.42	1.53	6%	1.08	1.50	5%	1.06
SAV B6	0.68	0.66	6%	0.97	BD			0.82	0.84	10%	1.03			

[a] Notes: (1) ATHO is used to calibrate efficiencies for 46.5Kev, 352Kev, and Dovelet for the rest. (2) Brancing ratios used are: 0.3721 for 352Kev of 214Pb; 00.277 for 911 of ^{228}Ac. (3) Rn degassing was checked by comparing samples sealed in epoxy with samples that were not. The two approaches give equivalent concentrations. (4) Using 338Kev for ^{228}Ac (not reported) gave equivalent concentrations within the counting uncertainties of the respective measurements. (5) (^{228}Ra) and (^{232}Th) activities calculated from mass spectrometry data (Table 2).

dances [*Workman et al.*, 2004] show an enrichment of the highly incompatible trace elements of 10 to 100x BSE, while the less incompatible elements are 1 to 10x BSE. BSE-normalized trace element patterns show depletions in Cs, Ba, U, K and Pb. The rejuvenated stage lava from Savaii, SAV B6, is an exception in showing no depletion in Ba.

[10] Basalts from the Samoan Islands characterize the enriched "EM2" end member, which is defined by radiogenic Sr, unradiogenic Nd, and moderate ^{206}Pb/^{204}Pb [*Zindler and Hart*, 1986]. The samples analyzed in this study show a wide, correlated range in ^{87}Sr/^{86}Sr and ^{143}Nd/^{144}Nd values (0.7044–0.7089, 0.51293–0.51251) and a narrow range of ^{206}Pb/^{206}Pb (19.24–19.40, excluding Savai'i SAV B6). Sample 78-1 from Malumalu Seamount has the most radiogenic ^{87}Sr/^{86}Sr (0.7089 [*Workman et al.*, 2004]) and until most recently it was the defining "EM2" end-member mantle component.

3. ^{238}U-, ^{235}U- and ^{232}Th-Decay Series Measurements and Their Implications for Sample Eruption Ages

[11] ^{238}U, ^{232}Th, ^{226}Ra, ^{210}Pb, ^{210}Po, ^{231}Pa, and ^{228}Ra concentrations and (^{234}U/^{238}U), (^{230}Th/^{232}Th), (^{230}Th/^{238}U), (^{226}Ra/^{230}Th), (^{228}Ra/^{232}Th) for the Samoan samples are reported in Tables 2–4 and shown in Figures 2–13. These nuclides concentrations, activities and isotopic ratios were measured by a combination of mass spectrometry, gamma

Notes to Table 2:

[a] Notes: (1) Replicate measurements designated A, B or Pa represent separate powder dissolutions. Numbered replicates represent different liquid aliquot splits of the same dissolution. (2) [U], [Th], [^{226}Ra] and [^{231}Pa] measured by ID-ICPMS at WHOI using the ThermoFisher ELEMENT2.( ) denotes activity. $\lambda 238 = 1.551 \times 10^{-10}$ yr^{-1}; $\lambda 232 = 4.948 \times 10^{-11}$ yr^{-1}; $\lambda 226 = 4.331 \times 10^{-4}$ yr^{-1}; $\lambda 231 = 2.115 \times 10^{-5}$ yr^{-1}; $\lambda 235 = 9.8485 \times 10^{-10}$ yr^{-1} [*Jaffey et al.*, 1971; *Le Roux and Glendenin*, 1963; *Holden*, 1990; *Tuli*, 2000; *Robert et al.*, 1969]. Measurement errors do not include uncertainties in $\lambda 238$ (0.07%), $\lambda 232$ (0.5%), $\lambda 226$ (0.4%), $\lambda 231$ (0.4%) or $\lambda 235$ (0.07%). See Appendix A for details of analytical methods. (3) Th isotopic compositions measured by: A) SIMS at WHOI using the Cameca IMS 1270 [*Layne and Sims*, 2000]; and B) MC-ICPMS at WHOI using the ThermoFisher NEPTUNE [*Ball et al.*, 2008; *Sims et al.*, 2008]. Activity ratios calculated using $\lambda 230 = 9.158 \times 10^{-6}$ yr^{-1} [*Cheng et al.*, 2000] and $\lambda 232 = 4.948 \times 10^{-11}$ yr^{-1} [*Le Roux and Glendenin*, 1963]; errors (2σ) range from: 0.4&–1% for both techniques and do not include uncertainties in $\lambda 230$ (0.4%) or $\lambda 232$ (0.5%). Replicates for rock standads analyzed for quality assurance were measured by Mc-ICPMS and were analyzed over the same time interval as the samples analyzed in this study. Comparison of WHOI's analyses of synthetic and rock standards are compared with results from other laboratories in *Sims et al.* [2008]. See Appendix A for details of analytical methods. (4) (^{234}U/^{238}U) measured by ICPMS at WHOI. $\lambda 234 = 2.826 \times 10^{-6}$ yr^{-1} [*Cheng et al.*, 2000], errors (2σ) < 0.5%; for these samples (^{234}U/^{238}U) = 1 within error, using an equilibrium ^{234}U/^{238}U atom ratio of 54.88 ppm. [*Cheng et al.*, 2000]. See Appendix A for details of analytical methods. (5) For (^{238}U/^{232}Th), (^{230}Th/^{232}Th) (^{230}Th/^{238}U), [^{226}Ra] and (^{226}Ra/^{230}Th), TML and ATHO were measured for quality assurance. Replicates represent seperate powder dissolutions. For (^{231}Pa/^{235}U) TML was used to calibrate ^{233}Pa spike. Two Hawaiian samples KL-31-KWWS-92 ans HK-04-KWWS-92 were measured for (^{231}Pa/^{235}U) quality assurance; these measurements agree within error with the reported values for these same samples in *Sims et al.* [1999].

Table 4. ^{210}Po Measurements by Alpha Spectroscopy[a]

	Date of Analysis	(^{210}Po), dpm/g	Rel Stdev (1σ)	(^{210}Po/^{226}Ra)
Alia101-01 (1)	7/18/2005	0.341	3.7%	
Alia101-01 (2)	6/6/2006	0.446	3.3%	
Alia101-01 (3)	9/27/2006	0.471	2.8%	0.69
63-13	12/2/2005	0.751	2.3%	0.74
63-13 (WHOI)	1999(WH)	0.770	2.0%	0.76
63-13 (WHOI)	2000(WH)	0.730	2.0%	0.72
68-30 (1)	12/2/2005	0.719	2.3%	
68-30 (2)	8/5/2006	0.736	2.4%	0.97
70-1	12/2/2005	0.833	2.2%	0.95
70-9	12/2/2005	0.861	2.5%	0.95
70-9 (WHOI)	1999(WH)	0.910	2.4%	1.00
71-2	12/2/2005	0.446	2.5%	0.96
72-2	12/25/2005	0.928	2.4%	0.99
73-1	3/6/2007	0.956	2.0%	0.94
73-3	12/25/2005	0.751	2.6%	0.77
73-12	1/9/2006	0.774	2.5%	0.93
78-1	12/25/2005	0.852	2.5%	0.97
RGM-1	1/9/2006	4.196	2.0%	

[a] Notes: ^{210}Po measured at University of Iowa, except for the few analyses from WHOI.

spectrometry and alpha spectrometry. Analytical details for these measurements are summarized in Appendix A and reported in other publications [*Layne and Sims*, 2000; *Choi et al.*, 2001; *Pichat et al.*, 2004; *Reagan et al.*, 2005; *Ball et al.*, 2008; *Sims et al.*, 2008].

[12] In the absence of secondary alteration, U-series disequilibria in volcanic rocks are attributed to chemical fractionations resulting from magmatic processes (e.g. melt generation and magma transport, crystal fractionation, or magma degassing). Since these fractionation processes ceased (i.e. the system became closed) before, at, or just after eruption, the presence of radioactive disequilibria places limits on the eruption ages. These limits are proportional to the half-life of the daughter isotope and must be considered maximum eruption ages because magma storage may also be involved.

[13] In this study we have measured several different ^{238}U, ^{235}U and ^{232}Th decay series nuclides having a wide range of half-lives (138 days to 75 ka) and differing chemical affinities (i.e. variable solid/melt and gas/melt partitioning). These U and Th decay series measurements provide age constraints on several important time windows: <350 ka; <150 ka; <8 ka; <100 a; <30 a; and, <2 a. The results of these U and Th decay series measurements and their implications for Samoan sample eruption ages are discussed below and summarized in Table 5.

3.1. ^{238}U Decay Series

3.1.1. ^{238}U–^{234}U

[14] ^{234}U/^{238}U was measured by Multi-Collector Inductively Coupled Plasma Mass Spectrometry (MC-ICPMS) using WHOI's ThermoFisher NEPTUNE [*Ball et al.*, 2008; *Sims et al.*, 2008]. Demonstrating that these samples' U and Th decay series disequilibria are not a result of secondary processes (namely seawater-rock interaction) is fundamental to their interpretation in terms of sample eruption ages and petrogenetic processes. All of the samples used in this study were fresh

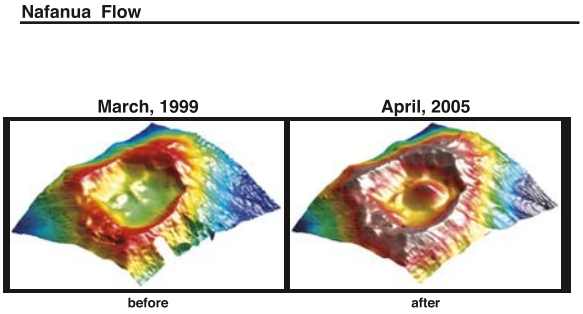

Figure 2. Bathymetric images of the summit crater of Vailuluu, showing the growth of the new volcanic cone Nafanua. The 1999 image is from swath-mapping during the AVON2/3 cruise of the R/V Melville [*Hart et al.*, 2000]; the 2005 image is from the ALIA cruise of the R/V Kilo Moana. Nafanua sits on the crater floor at ~1000 m, with a summit at 707 m [*Staudigel et al.*, 2006]. Perspective view courtesy of L. Montesi.

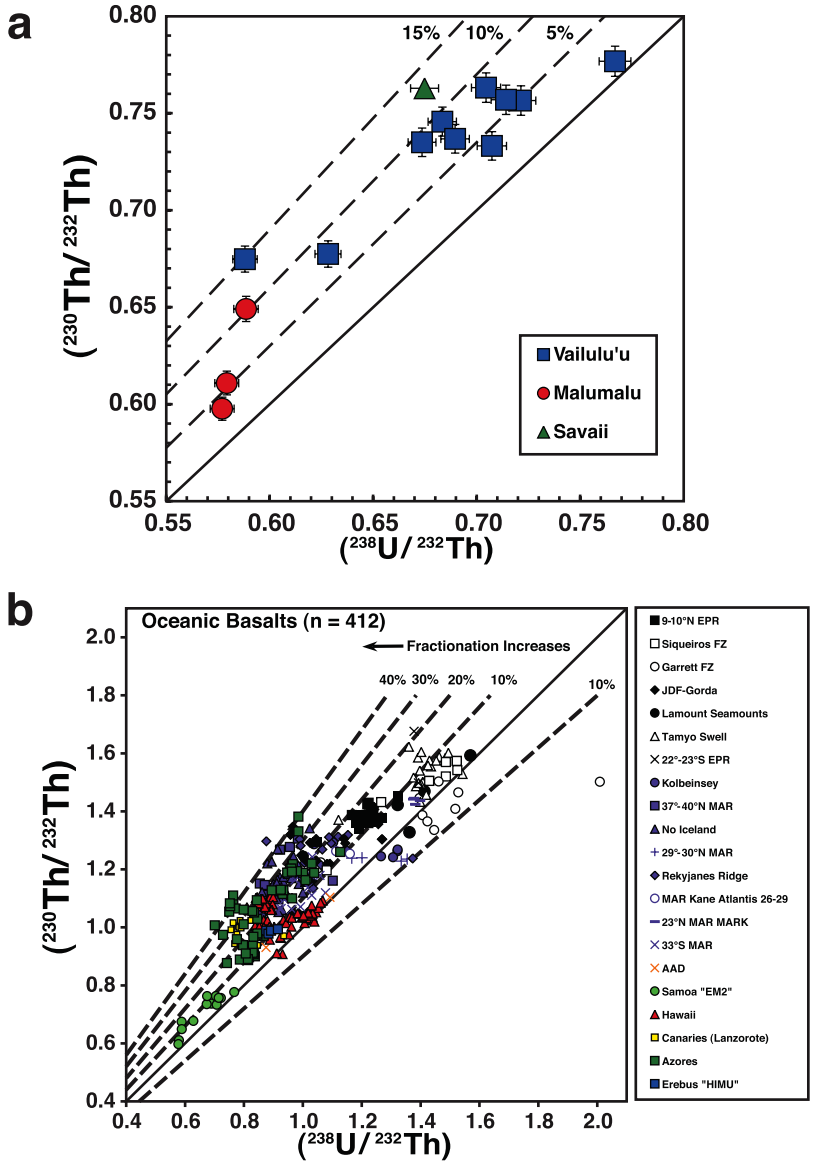

Figure 3. (^{230}Th/^{232}Th) versus (^{238}U/^{232}Th) for (a) young Samoan basaltic lavas measured in this study, and (b) a global compilation of literature data for mid-ocean ridge and ocean island basalts measured by mass spectrometric methods [*Bourdon et al.*, 1996a, 1996b; *Goldstein et al.*, 1989, 1993; *Lundstrom et al.*, 1995, 1998, 1999, 2003; *Peate et al.,* 2001; *Sims et al.*, 1995, 1999, 2001, 2002; *Sturm et al.*, 2000; *Tepley et al.*, 2004; *Cohen and O'nion*, 1993; *Pietruszka et al.*, 2001; *Stracke et al.*, 2003; *Kokfelt et al.*, 2003; *Sigmarsson et al.*, 1998; *Thomas et al.*, 1999; *Turner et al.*, 1997; *Claude-Ivanaj et al.*, 1998; *Widom et al.*, 1997; *Sims and Hart*, 2006]. The global data have been filtered to eliminate samples of uncertain eruption age, or altered by secondary, posteruptive processes. The solid dark line is the equiline, representing the secular equilibrium condition when the activity ratio of (^{230}Th/^{232}Th) equals (^{238}U/^{232}Th). If a mantle source has not been fractionated in the past ~350,000 years, it is constrained to lie along this equiline. Dashed lines are contours of (^{230}Th/^{238}U). For the Samoan samples, the relative measurement error (2σ), based on in-run statistics, is smaller than the size of the symbols (Table 2).

handpicked glasses (lightly leached prior to dissolution and analysis) and have (^{234}U/^{238}U) activity ratios (activity ratios are hereafter noted with parentheses) of unity (± 5 per mil), indicating minimal posteruptive alteration (Table 2). For the submarine basalts from Vailulu'u and Malumalu, (^{234}U/^{238}U) activity ratios are a sensitive indicator of seawater alteration, as seawater is significantly enriched in ^{234}U relative to ^{238}U (for seawater (^{234}U/^{238}U) = 1.14 ± 0.03 [*Ku et al.*, 1977; *Thurber*, 1962]). For young subaerial samples, such as the 1905 sample from Savaii, (^{234}U/^{238}U) of unity is a necessary but not sufficient condition for ruling out secondary alteration. However, this

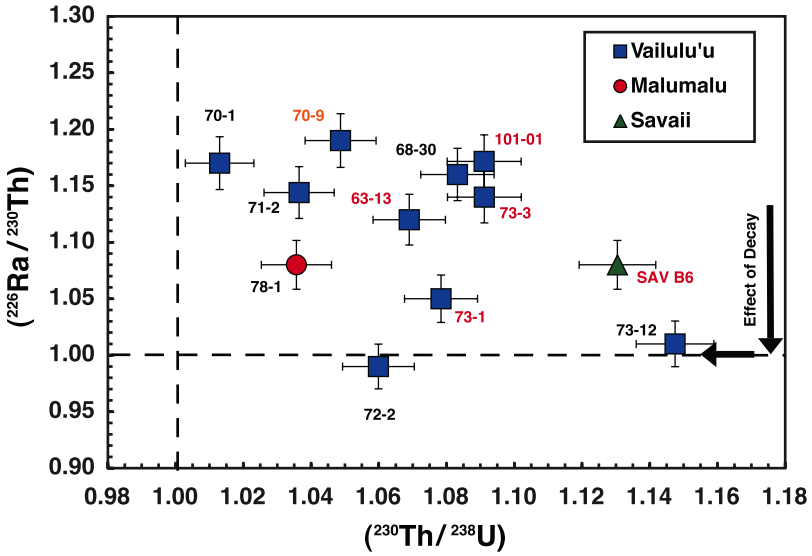

Figure 4. (^{226}Ra/^{230}Th) vs (^{230}Th/^{238}U) for the Vailulu'u, Malumalu and Savaii basalts. Red sample labels indicate young samples that have (^{210}Pb/^{226}Ra) < 1, or are historic (101-01; Savaii). Measurement errors are 2σ.

sample is from a young, historic flow, appeared fresh in hand specimen, and has $K_2O/P_2O_5 < 1$, and canonical Rb/Cs (102) and Ba/Rb (12.0) ratios, all indications of its pristine nature.

3.1.2. ^{238}U–^{230}Th

[15] ^{230}Th/^{232}Th was measured by Secondary Ionization Mass Spectrometry (SIMS) using WHOI's Cameca IMS 1270 [*Layne and Sims*, 2000], and by Multi-Collector Inductively Coupled Plasma Mass Spectrometry (MC-ICPMS) using WHOI's ThermoFisher NEPTUNE [*Ball et al.*, 2008; *Sims et al.*, 2008]. Th isotopic analyses were replicated several times. Reproducibility is within analytical errors (less than 1%).

[16] ^{238}U and ^{232}Th concentrations were measured by isotope dilution on a single collector sector ICPMS (ThermoFisher Element) at WHOI. Replicate values and averages are reported in Table 2.

[17] All fourteen Samoan samples have (^{230}Th/^{238}U) > 1 (hereafter referred to as ^{230}Th excesses) (Table 2 and Figure 3). The half-life of ^{230}Th is 75,690 ± 230 years [*Cheng et al.*, 2000], therefore these sample's ^{230}Th excesses require eruption ages of less than 300,000 years (Table 5). The large magnitude of these ^{230}Th excesses suggests even younger ages.

3.1.3. ^{230}Th–^{226}Ra

[18] ^{226}Ra ($t_{1/2}$ = 1599 ± 4 yrs [*Holden*, 1990]) was measured by both isotope dilution mass spectrometry using WHOI's ThermoFisher NEPTUNE and gamma counting of the short-lived ^{226}Ra daughters – ^{214}Pb and ^{214}Bi (Figures 4 and 5; Tables 2 and 3). This latter approach assumes that (^{226}Ra) is in radioactive equilibrium with (^{214}Pb) and (^{214}Bi), which is reasonable given the extremely short half-lives for these daughter nuclides in this part of the ^{238}U decay series (35 msec to 3.83 days). Within their respective analytical uncertainties, both daughter activities give concurrent results amongst themselves and with the mass spectrometric measurements (Figure 5).

[19] For the 12 Samoan samples analyzed, two (72-2; 73-12) have (^{226}Ra/^{230}Th) = 1 (Figures 4 and 5; Tables 2 and 3); the other 10 samples have (^{226}Ra/^{230}Th) > 1 (hereafter referred to as ^{226}Ra excess). These 10 samples' significant ^{226}Ra excesses indicate eruption ages of less than 8 ka (Table 5).

3.1.4. ^{226}Ra–^{210}Pb

[20] ^{210}Pb ($t_{1/2}$ = 22.6 ± 0.1 yrs [*Holden*, 1990]) was determined directly by gamma spectroscopy and by ^{210}Po ingrowth using alpha spectrometry (Figure 6; Tables 3 and 4). The ^{210}Po alpha counting data is more precise and accurate and therefore we only consider this data for determining eruption ages.

[21] Four samples from the Vailulu'u summit crater (73-1; 73-3; 63-13; ALIA 101-01) all have (^{210}Pb/^{226}Ra) < 1 (hereafter referred to as ^{210}Pb deficits), while all other samples are in equilibrium within analytical uncertainties. The significant ^{210}Pb deficits measured in these four samples indicate their eruption ages are less than 100 yrs (Table 5).

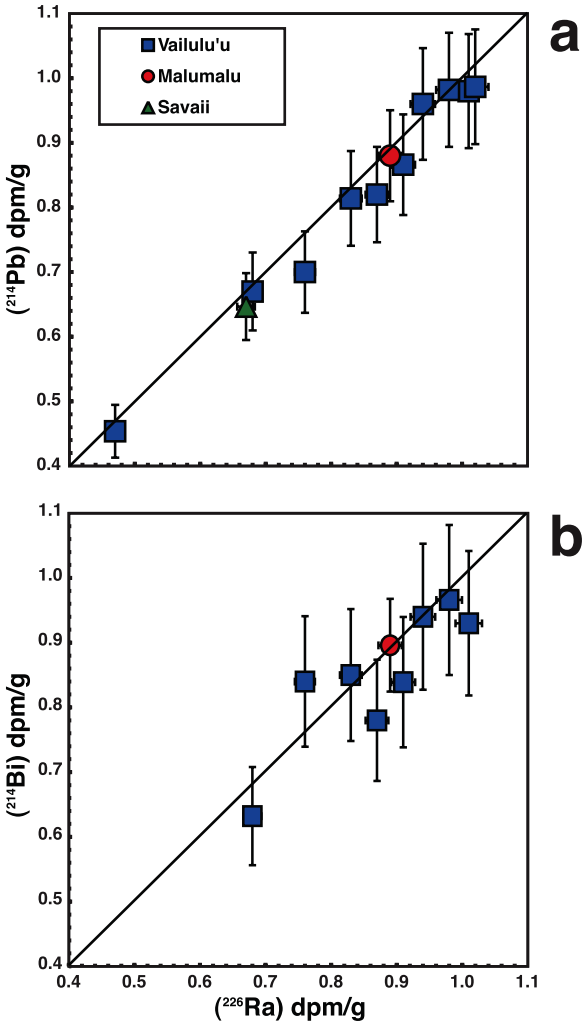

Figure 5. ^{226}Ra (dpm/g) measured by isotope dilution mass spectrometry versus (a) ^{214}Pb (dpm/g) and (b) ^{214}Bi (dpm/g) measured by gamma spectroscopy. For ^{226}Ra measured by isotope dilution, error bars represent cumulative uncertainties associated with spike calibration and instrument reproducibility; for ^{214}Pb and ^{214}Bi gamma measurements, error bars represent 2σ counting errors. Within analytical uncertainties, (^{214}Pb) and (^{214}Bi) are in radioactive equilibrium with (^{226}Ra); this is to be expected given the extremely short half-lives of the intervening ^{226}Ra daughter nuclides of the ^{238}U decay chain (see text for details). The agreement of these two types of data, which have different sources of error, validates the accuracy of both measurements.

3.1.5. ^{210}Pb–^{210}Po

[22] For sample ALIA 101-1, from the newly mapped Nafanua cone in the summit crater of Vailulu'u (Figure 2), ^{210}Po ($t_{1/2}$ = 138.4 ± 0.1 days [*Holden*, 1990]) was measured by alpha-spectrometry in three aliquots over a one-year period (Table 4). The eruption age was determined by best-fit regression to a radioactive ingrowth curve (Figure 7). In most erupted magmas, complete polonium volatilization during eruption creates an initial ^{210}Po deficit relative to the ^{210}Pb grandparent; this is subsequently erased with time via radioactive ingrowth towards secular equilibrium [e.g., *Bennett et al.*, 1982; *Gill et al.*, 1985; *Reagan et al.*, 2008]. Using the two sigma uncertainties on the ^{210}Po analyses (Table 4) we calculate an eruption date for ALIA 101-1 of November 8, 2004 (+62/−67 days), assuming that (^{210}Po) = 0 at the time of eruption. This assumption of 100% Po degassing is supported by analyses of a shallow submarine sample from Macdonald seamount that was entirely degassed on the date of sample collection (presumed eruption), whereas Po degassing at greater depth (>3 km) is presently constrained to 75–100% [*Rubin*, 1997; *Rubin et al.*, 1994]. Incomplete Po degassing would cause reported ages to be overestimates, and so the reported age is nominally a maximum.

[23] ^{210}Po was also measured on two Vailulu'u samples (70-9, 63-13) soon after their collection in 1999, and then again in late 2000 (by A. Fleer, at WHOI). These measurements are similar to the University of Iowa's 2005 results indicating that they were clearly in equilibrium with respect to

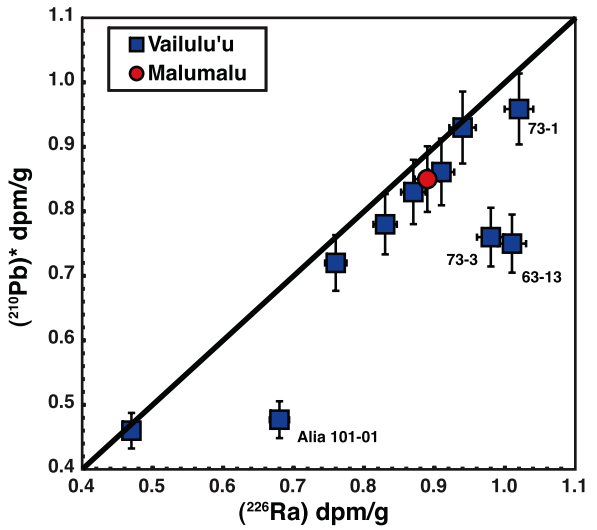

Figure 6. (^{210}Pb)* versus ^{226}Ra (dpm/g), where (^{210}Pb)* is determined from the activity of ^{210}Po, assuming (^{210}Po) = (^{210}Pb). For ^{226}Ra measured by isotope dilution, error bars represent cumulative uncertainties associated with spike calibration and instrument reproducibility; for ^{210}Po determined by alpha spectroscopy, error bars represent 2σ counting uncertainties. Only four samples, all from the summit crater of Vailuluu, have significant (^{210}Pb) deficiencies relative to (^{226}Ra).

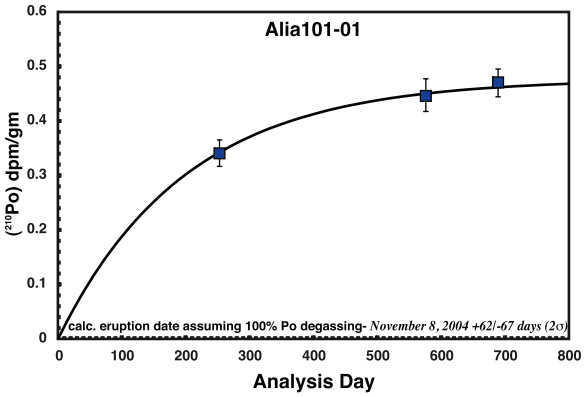

Figure 7. ^{210}Po ingrowth curve for ALIA 101-01. Eruption age is determined by assuming 100% degassing of Po in the initial lava and extrapolating the best-fit radioactive equilibration curve through the data. Error in the calculated maximum age is determined by regression through the data at the limits of their 2-sigma analytical errors.

(^{210}Po/^{210}Pb) when first measured and thus older than 2 years.

3.2. ^{232}Th Decay Series

3.2.1. ^{232}Th–^{228}Ra

[24] As a proxy for ^{228}Ra ($t_{1/2}$ = 5.75 ± 0.03 yrs [*Holden*, 1990]), we measured ^{228}Ac and ^{208}Tl by gamma spectroscopy in eleven samples (Figure 8 and Table 3). The ^{228}Ac proxy assumes that (^{228}Ra) is in radioactive equilibrium with its daughter (^{228}Ac), which is a reasonable assumption given the extremely short half-life of ^{228}Ac ($t_{1/2}$ = 6.13 hrs). The ^{208}Tl proxy assumes that (^{228}Ra) is in radioactive equilibrium all the way down the chain to its distant granddaughter (^{208}Tl), which is also reasonable since the half-lives of these different nuclei range from less than 1 microsecond to 3.6 days.

[25] All samples have (^{228}Ac/^{232}Th) and (^{208}Tl/^{232}Th) in radioactive equilibrium to within 1-sigma counting uncertainties (Figure 8), and thus, by inference, they are in equilibrium with respect to (^{228}Ra/^{232}Th). All of these samples except ALIA 101-01 were collected in 1999 and counted for ^{228}Ac in late 2005/early 2006, so one half-life had elapsed between collection and measurement. For ALIA 101-01, the sample was counted within one year of its collection. The large uncertainties in the ^{228}Ra measurement (4–10%) limit the age resolution of this technique to about 15 years. For most of these samples, the measured (^{228}Ra/^{232}Th) of unity could be, in part, a function of the time between collection and counting. However, for ALIA 101, this is not the case, and so its (^{228}Ra/^{232}Th) of unity suggests that either: (1) (^{228}Ra/^{232}Th) was never out of equilibrium in these samples, which is unlikely based on the observed ^{226}Ra excesses over ^{230}Th; or, (2) any (^{228}Ra/^{232}Th) disequilibria produced during melting decayed away prior to eruption as magmas migrated to the surface over a period exceeding 30 years [*Reagan et al.*, 1992].

3.3. ^{235}U Decay Series

3.3.1. ^{235}U–^{231}Pa

[26] ^{231}Pa concentrations were measured by isotope dilution on a single collector sector ICPMS (ThermoFinnigan Element) at WHOI. (^{231}Pa/^{235}U) is greater than one in all four of the Samoan

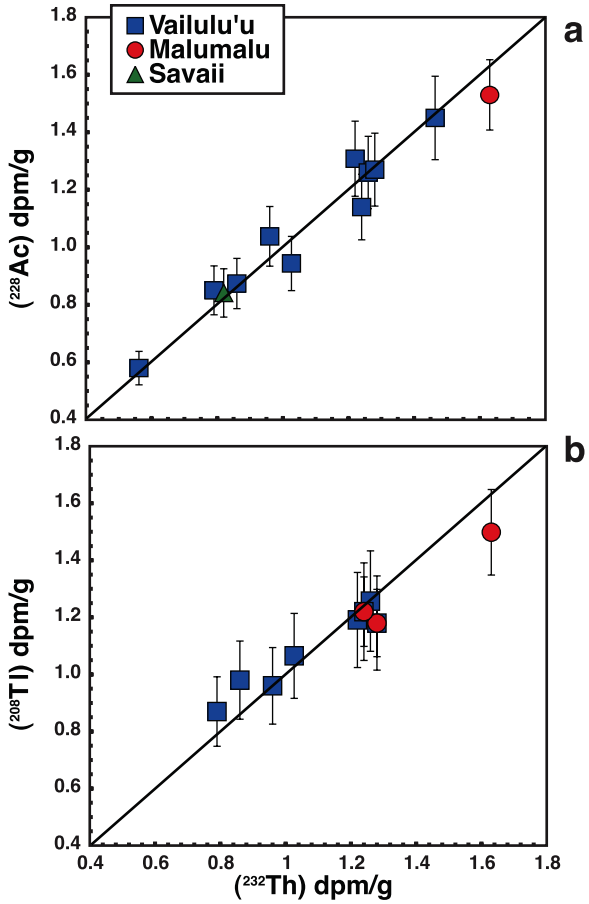

Figure 8. ^{232}Th (dpm/g) measured by isotope dilution mass spectrometry versus (a) ^{228}Ac (dpm/g) and (b) ^{208}Tl (dpm/g) measured by gamma spectroscopy. ^{228}Ac and ^{208}Tl are measured as a proxy for ^{228}Ra, which these data indicate are in equilibrium, within error, with ^{232}Th (see text for details). Error bars on ^{228}Ac and ^{208}Tl represent 2σ counting uncertainties (Table 3).

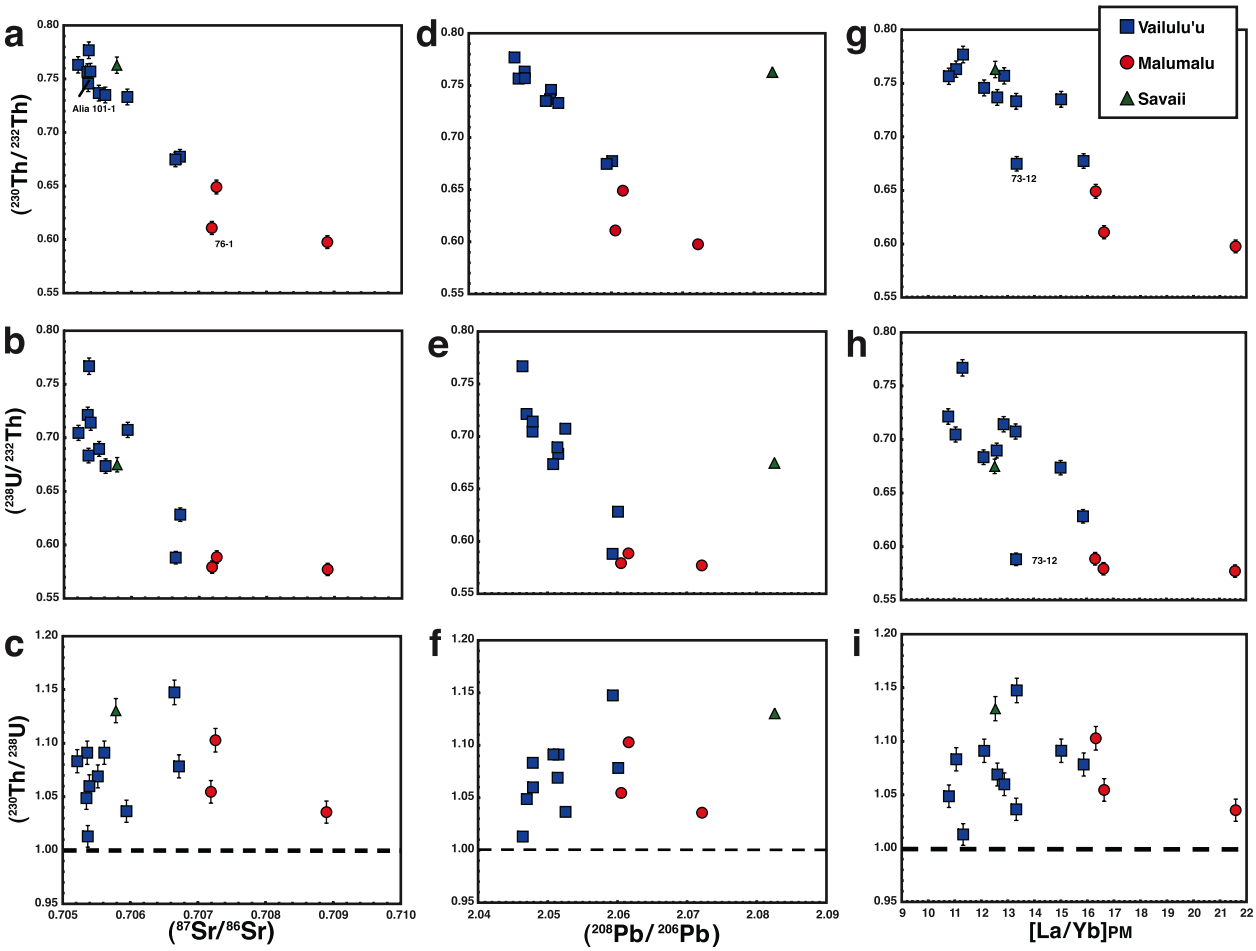

Figure 9. (a–i) (^{230}Th/^{232}Th), (^{238}U/^{232}Th) and (^{230}Th/^{238}U) versus ^{87}Sr/^{86}Sr, ^{208}Pb/^{206}Pb and primitive upper mantle normalized La/Yb for young Samoan basaltic lavas. Isotope and trace element concentrations are from *Workman et al.* [2004]. Primitive upper mantle values used to normalize La/Yb are taken from *McDonough and Sun* [1995].

samples measured, indicating that ^{231}Pa is enriched relative to ^{235}U (Table 3). These ^{231}Pa excesses require maximum eruption ages of less than 150 Ka (Table 5). The large magnitude of these ^{231}Pa excesses suggests even younger ages, probably less than the half-life of ^{231}Pa ($t_{1/2}$ = 32,760 ± 220 yrs [*Robert et al.*, 1969]). This age constraint is consistent with three of these four samples having ^{226}Ra excesses, which infer even younger eruption ages (<8 Ka).

4. Implications of Age Constraints for Magma Production and Eruption Rates at Vailulu'u and Malumalu

[27] For the submarine volcano Vailulu'u, the determined U-series ages are for lavas from both the summit crater and lower rift zones (Figure 1). All ten Vailulu'u samples show significant (^{230}Th/^{238}U) disequilibria, requiring their eruption ages be less than 300,000 years; of these, eight have (^{226}Ra/^{230}Th) > 1 indicating that their eruption ages are < 8 ka; and, all four lavas within the summit crater have (^{210}Pb/^{226}Ra) < 1, indicating that their eruption ages are less than 100a. These ages indicate that Vailulu'u is currently active and magmatically productive with young lavas resurfacing both its summit crater and deeper rift zones.

[28] Within the summit crater, observational evidence and U-series ages indicate at least 4 recent eruptive episodes. The youngest documented eruption is the Nafanua cone (ALIA 101), collected in April 2005, and whose Po ingrowth eruption date is calculated to be about November 8, 2004 (Figures 2 and 7). Three of the samples collected in March 1999 (63-13, 73-1 and 73-3) have ^{210}Pb deficits, so their ages are inferred to be pre-March 1999, but less than 100 a. Four samples (70-9, 70-1, 68-30, 73-12)

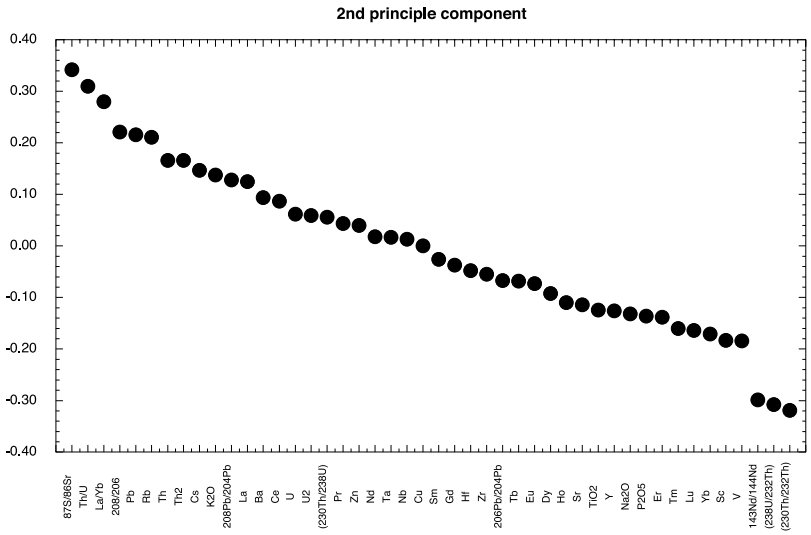

Figure 10. Second principal components for the Samoan samples, including isotopic ratios and a few selected trace-element ratios. 78% of the chemical and isotopic variability in the Samoan data set can be explained by the first two principal components. The first principal component (not shown) accounts for 60% of the variance in the data and is interpreted as reflecting the effects of fractional crystallization, namely the removal and addition of olivine. The second principle component (shown here) accounts for an additional 18% of the data variance. Principle component analysis assumes a linear relationship among the variables. Correlations among ($^{238}U/^{232}Th$) ($^{230}Th/^{232}Th$) and long-lived isotope ratios like $^{87}Sr/^{86}Sr$ and $^{143}Nd/^{144}Nd$ are not linear across the global oceanic data set [*Sims and Hart*, 2006], and even show some curvature amongst this Samoan data set (Figure 9), namely because of the enriched end-member 78-1. Nonetheless, the strong covariance among the lavas' isotopic compositions and trace element abundances clearly reflects the influence of source variability.

have ^{226}Ra excesses, but ($^{210}Pb/^{226}Ra$) is in equilibrium, so their ages are inferred to be >100a and <8 ka. Finally, 73-12 is in equilibrium with respect to ($^{226}Ra/^{230}Th$) and ($^{210}Pb/^{226}Ra$), so its eruption age is inferred to be >8 ka (note that this is true also of 72-2, from the deep NE Rift). While we have binned these U-series ages into four temporal episodes, all of the summit crater samples have distinctly different Nd, Sr and Pb isotopic signatures [*Workman et al.*, 2004] suggesting either: (1) they come from different eruptions, implying more than four eruption episodes; or, (2) intralava isotopic variability is large (intradredge variability is demonstrably large; e.g. compare the three dredge 73 samples). Only the recent Nafanua cone sample (101-01) and the NE rift sample (72-2) have indistinguishable Sr, Nd and Pb isotopic signatures, yet these differ in eruption age by at least 8,000 years. It is likely that all of the analyzed Vailulu'u samples have come from different eruptions.

[29] On Malumalu, all three samples (76-1, 77-9, 78-1) have ^{230}Th excesses, sample 76-1 also has a ^{231}Pa excess and sample 78-1 also has a ^{226}Ra excess. These disequilibria indicate that there has been magmatic activity on Malumalu more recently than 8 ka, at least two eruptions in the last 150 Ka, and at least three eruptions in the past 300 ka.

[30] The maximum eruption ages we have determined from U– and Th– decay series measurements indicate that the surfaces of Vailulu'u and Malumalu are quite young and that Vailulu'u has erupted several times over the past 100 yrs, including in 2004. These young ages are consistent with the hypothesis that these volcanoes represent the leading edge of the Samoan plume [*Hart et al.*, 2000, 2004; *Staudigel et al.*, 2004].

5. Implications for the Drift of the Samoan Plume

[31] It is apparent from the data presented above that volcanism is to some extent coeval on Malumalu and Vailulu'u seamounts (Table 5). The linear distance between these two volcanoes is 90 km and they lie on distinctly separate en echelon volcanic

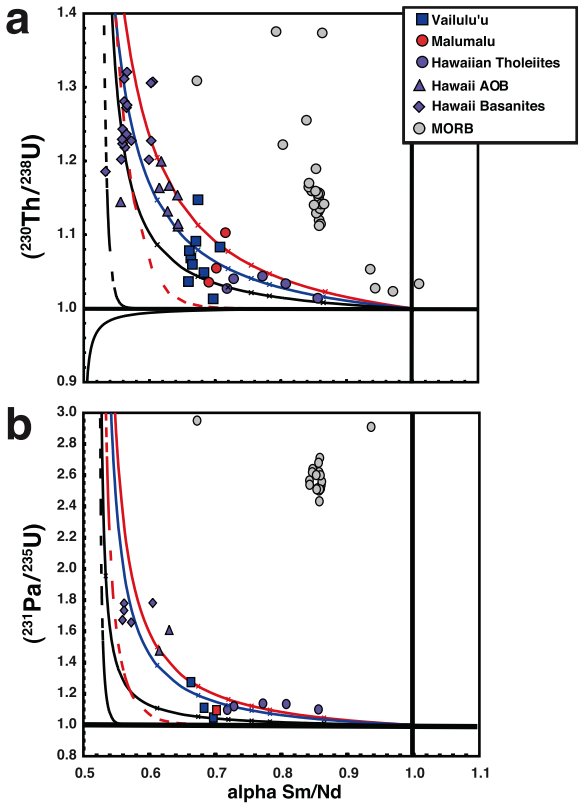

Figure 11. $\alpha_{Sm/Nd}$ versus (a) ($^{230}Th/^{238}U$); and (b) ($^{231}Pa/^{235}U$) for Samoan, Hawaiian and MORB basalts. Solid lines represent batch-melting, and the dashed lines represent accumulated fractional melting of a garnet lherzolite source (12% garnet, 8% clinopyroxene, 21% orthopyroxene, 59% olivine), using the equations given in *Shaw* 1970. Different colors represent constant D_{Nd} = 0.02 and D_{Sm} = 0.04 [*McKay*, 1989; *Salters et al.*, 2002], but different values of D_U, D_{Th} and D_{Pa}. In 11a, the red lines use D_U = 0.0052 and D_{Th} = 0.0026 [*Salters and Longhi*, 1999]; the black lines use D_U = 0.0012 and D_{Th} = 0.0003 [*Beattie*, 1993a, 1993b]; and the single blue line represents the inverted batch melting trend (see text for details), for which we calculate D_U = 0.0038 and D_{Th} = 0.0021. The black line below ($^{230}Th/^{238}U$) = 1.0 is for spinel facies melting. In 11b, D_{Nd} = 0.02, D_{Sm} = 0.04 [*McKay*, 1989] and D_{Pa} is assumed to be 1E-5 (see text for details); the red line uses D_U = 0.0052 [*Salters and Longhi*, 1999]; the black lines use D_U = 0.0012 [*Beattie*, 1993a, 1993b]. The single blue line represents the inverted batch melting trend for the combined Samoan and Hawaiian data suites (see text for details), for which we calculate D_U = 0.004 and D_{Pa} = 0.00009. In both cases, MORB lie well above of the simple batch-melting trend observed for the Hawaiian and Samoa data and require complex melting scenarios incorporating ingrowth of daughter nuclides, multiple porosities, mixing of polybaric melts and variable cpx:garnet source ratios [*Sims et al.*, 1995, 1999, 2002; *Bourdon et al.*, 1998; *Bourdon and Sims*, 2003; *Lundstrom et al.*, 1995; *Lundstrom*, 2000]. Increments of melting (10%, 5%, 4%, 3%, 2%, 1%) are shown by crosses.

lineaments (Figure 1). Malumalu anchors the east end of a long submarine lineament running SE from Tutuila, whereas Vailulu'u is the beginning of a new lineament lying NE of the intervening Muli-Ta'u lineament. There is also minor young (coeval) volcanism on Ta'u and Ofu-Olosega (the orthogonal distance between the Malumalu and Ta'u lineaments is 66 km). *Hart et al.* [2004] proposed that the Samoa plume is being blown to the NE by mantle flow escaping from underneath the subducting Tonga slab during its eastward roll-back. The present demonstration of young coeval volcanism on Malumalu and Vailulu'u provides a strong measure of support for this hypothesis. While the plumbing system of the plume currently appears to be feeding both volcanoes, this model predicts that volcanism on Malumalu will wane over the next 10^4–10^5 years while increasing in vigor on Vailulu'u.

6. Basalt Petrogenesis Beneath Samoa

6.1. Comparison of $^{230}Th/^{238}U$, $^{231}Pa/^{235}U$ and $^{226}Ra/^{230}Th$ Data With Melting Models

[32] The daughter isotopes ^{230}Th and ^{226}Ra (^{238}U-decay series) and ^{231}Pa (^{235}U-decay series) have half-lives which encompass the time-scales over which melting and melt extraction are thought to occur. While secular equilibrium requirements constrain their mantle abundances and activities, differences in solid/liquid partitioning of U, Th, Pa and Ra produce significant parent-daughter fractionations during melting, perturbing this secular equilibrium. Therefore, measurement of disequilibria among the U-series radioisotopes can provide unique and direct constraints on the timing and extent of chemical fractionations that occur during magma genesis.

[33] In the following, we compare the ($^{230}Th/^{238}U$), ($^{226}Ra/^{230}Th$) and ($^{231}Pa/^{235}U$) of Samoan lavas to forward models of melt generation and magma transport. We consider both: (1) 'time-independent melting' in which parent/daughter fractionation is attributed to low melt fractions during 'batch' or 'fractional' melting; and, (2) 'time-dependent melting' which incorporates daughter isotope ingrowth and decay over the timescales of melt generation and magma transport. There are now several models relating the isotope systematics of U-series disequilibria to the timescales of the melting process [e.g., *McKenzie*, 1985; *Spiegelman and Elliot*, 1993; *Williams and Gill*, 1989; *Iwamori*, 1994; *Qin*, 1992; *Lundstrom*, 2000; *Richardson and McKenzie*, 1994; *Jull et al.*, 2002]. These models

differ mainly in their treatment of the melt extraction process (i.e. reactive porous flow versus near-fractional melting), however, because they incorporate the effect of radioactive ingrowth and decay of the daughter isotopes during melt production, they are able to predict mantle melting rates and melt transport rates based upon U-Th-Ra and U-Pa disequilibria. These U-series mantle melting rates can, in turn, be combined with theoretical predictions of melt productivity [e.g., *Asimow et al.*, 1997; *McKenzie and Bickle*, 1988] to calculate a model solid mantle upwelling rate [*Sims et al.*, 1999; *Pietruszka et al.*, 2001; *Bourdon and Sims*, 2003; *Kokfelt et al.*, 2003; *Bourdon et al.*, 2006].

[34] Interpretation of U- and Th- series disequilibria data in terms of magmatic processes requires explicit knowledge of eruption ages relative to the half-life of the relevant system. As discussed above, the Vailulu'u and Malumalu basalts are all submarine samples and so the only constraints on their eruption ages (except ALIA 101-01) are from the U-series disequilibria measurements (Table 5). The presence or absence of disequilibria in the shorter-lived systems can be used as an age filter when interpreting the longer-lived disequilibria data. For our interpretation of (^{230}Th/^{238}U) and (^{231}Pa/^{235}U), only the 10 samples with (^{226}Ra/^{230}Th) > 1 are considered (Figure 4), as their ages are inferred to be <8 ka and their U-Th and U-Pa disequilibria thus unperturbed by posteruptive decay (within analytical uncertainties). For our interpretation of (^{226}Ra/^{230}Th), only the 4 samples with (^{210}Pb/^{226}Ra) < 1 are considered (Figure 6), as their eruption ages are inferred to be less than 100 a and thus their ^{226}Ra excess can be considered unperturbed by posteruptive decay.

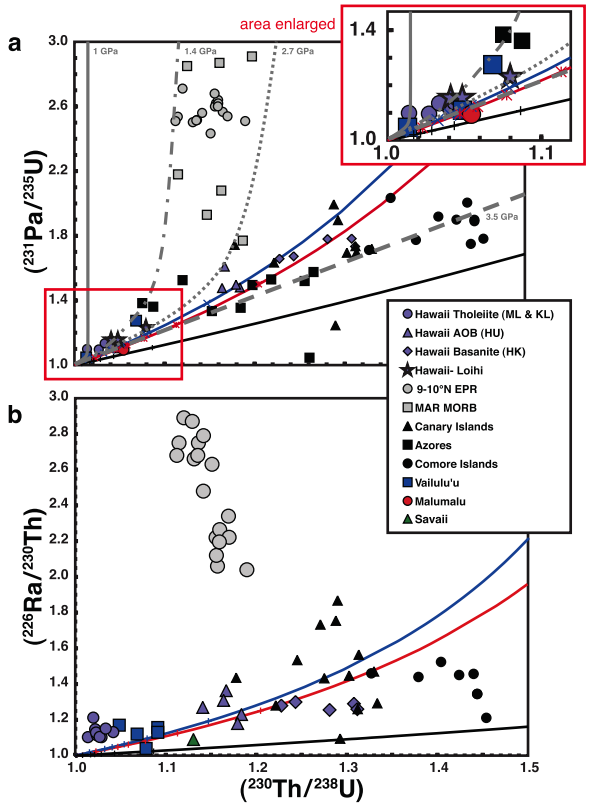

Figure 12. (^{230}Th/^{238}U) versus (a) (^{231}Pa/^{235}U) and (b) (^{226}Ra/^{230}Th) for a compilation of OIB and MORB data compared with simple batch melting models. The D_U, D_{Th} and D_{Pa} values and respective color scheme, for the different lines are the same as given in Figure 11, except for D_{Ra}, which is held constant and assumed to be 4E-5 in all cases. Also shown in 12a, are the recent partitioning data of *Landwehr et al.* [2001] as a function of pressure (light grey curves). As discussed by *Bourdon and Sims* [2003], the distinction between MORB and OIB can be explained by a variable cpx/garnet ratio in the mantle source, determined by the initial pressure of melting. The OIB data lie along melting trends that are consistent with melting at a pressure above the garnet-spinel transition, and having a low cpx/garnet ratio. In contrast, MORB can be produced by a shallower average depth of melting, and are characterized by larger ^{231}Pa excess at a given ^{230}Th/^{238}U. In Figure 12b, the ^{226}Ra excesses for all OIB are smaller than MORB and also tend to be positively correlated. For MORB, the only sample suite whose ages are known to be young relative to the half-life of ^{226}Ra are from 9-10°N EPR [*Sims et al.*, 2002]. These MORB samples show an inverse correlation between ^{230}Th excess and ^{226}Ra excess (as well as major and trace element composition) which was interpreted as mixing of two types of melt: one having a high ^{230}Th component equilibrated with deep, un-depleted garnet peridotites (>70 kms); the other having a high ^{226}Ra component preserving characteristics indicative of equilibration with highly depleted, residual harzburgite in the uppermost, spinel facies mantle (<70 kms). More recent interpretations [*Faul*, 2001; *Saal and Van Orman*, 2004] debate the mechanisms responsible for the large ^{226}Ra excesses in MORB, but not its shallow origin.

6.1.1. ^{238}U–^{230}Th

[35] The (^{230}Th/^{238}U) of the measured Samoan basalts are greater than one, indicating that ^{230}Th has been enriched in the melt relative to its parent ^{238}U. These ^{230}Th excesses indicate that garnet is required as a residual phase in the mantle source [*Beattie*, 1993a, 1993b; *La Tourrette and Burnett*, 1992; *La Tourrette et al.*, 1993; *Hauri et al.*, 1994; *Lundstrom et al.*, 1994; *Salters and Longhi*, 1999]. High-pressure, near-solidus clinopyroxene can also produce (^{230}Th/^{238}U) somewhat greater than one

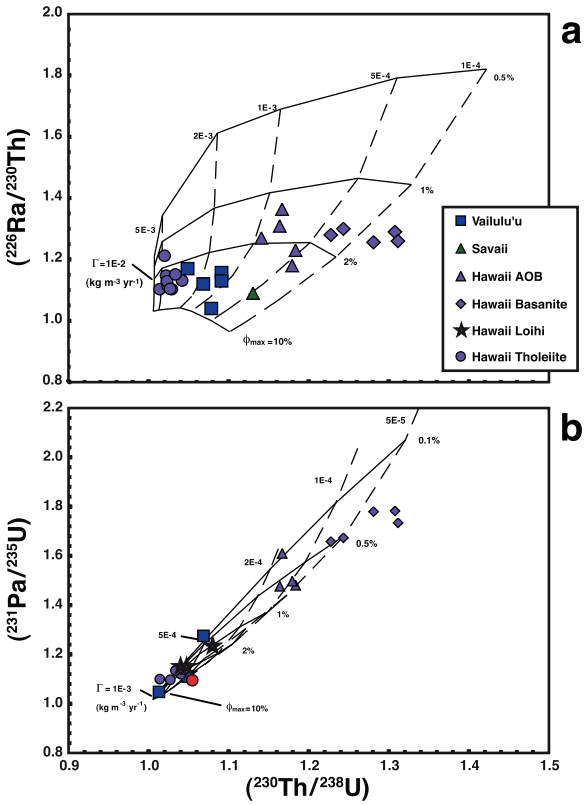

Figure 13. (^{230}Th/^{238}U) versus (a) (^{226}Ra/^{230}Th) and (b) (^{231}Pa/^{235}U) for Samoan and Hawaiian data compared with chromatographic porous flow models. In the chromatographic melting models, assumptions regarding the length and depth-porosity profile of the melt column have significant effects on calculated melting rates and porosities. For the chromatographic melting grid shown here, we use the analytical approximation of the *Spiegelman and Elliot* [1993] model, as given by *Sims et al.* [1999], a melting column of 50 kms, D_U and D_{Th} from *Salters and Longhi* [1999] and an inferred D_{Ra} of 4E-5 and D_{Pa} of 1E-5. The horizontally trending solid lines show activity ratios for constant maximum porosity (f_{max}) in percent, while the vertically trending dashed lines show the activity ratios for a constant melting rate in kg m^{-3} yr^{-1}. This analytical approximation gives results similar to the full numerical solution. However, because the analytical solution assumes a constant porosity throughout the melt column, whereas the numerical solutions (see e.g. User Calc) infer an upward increasing porosity (to keep melt flux constant), the porosities inferred from the analytical solution are higher than those derived by the numerical solution, for a given ^{226}Ra excess. These differences in calculated melting rates are most significant for larger Th and Ra excesses, but are negligible for the range of disequilibria observed for Samoa.

[*Landwehr et al.*, 2001], however, the large excesses seen in most oceanic basalts (both MORB and OIB) requires garnet as a residual phase during melting. A deep garnet-bearing source for these basalts is also indicated by the silica-undersaturated alkaline compositions, high FeO contents, fractionated HREE ratios (Dy/Yb ranges from 1.7–2.3) and the age and thickness of the Samoan lithosphere (68–72 kms; M. Jackson and J. Collins, personal communication).

[36] (^{230}Th/^{232}Th) and (^{238}U/^{232}Th) of the Samoan basalts are the lowest yet measured in oceanic basalts, suggesting that they come from a source with high Th/U (Figure 3). (^{230}Th/^{232}Th) and (^{238}U/^{232}Th) are variable and well correlated with ^{87}Sr/^{86}Sr, ^{143}Nd/^{144}Nd and ^{208}Pb/^{206}Pb; these correlations indicate that the high Th/U ratio of the Samoan source is a long-lived feature, consistent with the enrichment of Rb/Sr, Nd/Sm and Th/U in the lavas (Figures 9 and 10). The Samoan samples extreme (^{230}Th/^{232}Th) and (^{238}U/^{232}Th) also change the functional form (from linear to hyperbolic) of the oceanic basalt global arrays [*Sims and Hart*, 2006]. (^{230}Th/^{232}Th) and (^{238}U/^{232}Th) are also well correlated with incompatible trace element ratios like La/Yb (Figures 9 and 10). These correlations between (^{230}Th/^{232}Th), (^{238}U/^{232}Th), La/Yb and ^{87}Sr/^{86}Sr, and ^{143}Nd/^{144}Nd and ^{208}Pb/^{206}Pb indicate that long-term source heterogeneity is exerting a primary influence on the measured trace element abundances of these samples.

[37] The (^{230}Th/^{238}U) excesses are limited in range and extent and show no systematic variation with either long-term source characteristics (e.g. ^{87}Sr/^{86}Sr, ^{143}Nd/^{144}Nd, ^{206}Pb/^{204}Pb) or trace element ratios and abundances (e.g. La/Yb) (Figures 9

Table 5. Eruption Age Limits Based on U-Series Measurements

Sample	Maximum Eruption Ages	Constraining System
Alia 101-01	11/08/04 (+62/−67 days)	^{210}Pb-^{210}Po
63-13	<100a	^{226}Ra-^{210}Pb
68-30	<8ka	^{230}Th-^{226}Ra
70-1	<8ka	^{230}Th-^{226}Ra
70-9	<8ka	^{230}Th-^{226}Ra
71-2	<8ka	^{230}Th-^{226}Ra
72-2	<350Ka	^{238}U-^{230}Th
73-1	<100a	^{226}Ra-^{210}Pb
73-3	<100a	^{226}Ra-^{210}Pb
73-12	<350Ka	^{238}U-^{230}Th
76-1	<150ka	^{235}U-^{231}Pa
77-9	<350Ka	^{238}U-^{230}Th
78-1	<8ka	^{230}Th-^{226}Ra
SAV B6	1901	historic

and 10). However, correlations between (^{230}Th/^{238}U) and other trace element ratios such as La/Yb are not necessarily expected. The Samoan lavas are all alkaline basalts derived by similar extents of mantle melting, so trace element variations induced by differences in degree of melting will be small compared to the large variability inherited from the source [*Sims and Hart*, 2006; *Workman et al.*, 2004]. This is in marked contrast to OIB suites, like Hawaii, where there is a large range of basalt compositions (from tholeiites to basanites) and the (^{230}Th/^{238}U) varies systematically as a function of the extent of melting, as inferred from major and trace-element abundances [*Sims et al.*, 1995, 1999].

[38] Because the source ratio is not known for most trace element pairs, it is difficult to quantify the amount of chemical fractionation occurring during basalt petrogenesis. However, for trace element ratios that are part of an isotopic system (such as Sm/Nd, Lu/Hf, Rb/Sr, U/Pb and Th/Pb), isotopic abundances can be used to constrain these elemental ratios in the magma source [*DePaolo*, 1988; *Salters*, 1996; *Salters and Hart*, 1989; *Sims et al.*, 1995, 1999; *Stracke et al.*, 1999; *Workman and Hart*, 2005; *Workman et al.*, 2004]. Typically, Sm-Nd and Lu-Hf are preferred because the behaviors of these elements during basalt petrogenesis are relatively well understood [*DePaolo*, 1988; *McKay*, 1989; *Salters and Hart*, 1989; *Sims et al.*, 1995; *Salters et al.*, 2002]. With long-lived isotope systems like Sm-Nd or Lu-Hf, estimation of elemental source ratios is limited by uncertainties in our knowledge of the mantle source age, whereas in the ^{238}U–^{230}Th system, the source ratio is known explicitly from secular equilibrium constraints.

[39] To evaluate (^{230}Th/^{238}U) of the Samoan basalts in terms of simple 'time-independent' melting models, we compare Th/U fractionation, inferred from (^{230}Th/^{238}U), with Sm/Nd fractionation, as represented by $\alpha_{Sm/Nd}$, where $\alpha_{Sm/Nd}$ = (Sm/Nd)$_{magma}$/(Sm/Nd)$_{source}$ [cf. *DePaolo*, 1988; *Sims et al.*, 1995] (Figure 11a). To calculate the Sm/Nd source ratio we use a 1.8 Ga isochron (age of the NHRL [*Hart*, 1984]) and assume that the depleted mantle and continental crust are complementary derivatives of the bulk silicate earth. While the age and pedigree of the Samoan source are debatable, the values we have calculated for the Samoan source are comparable to the EM2 source value calculated by *Workman et al.* [2004], using different assumptions and model ages. By themselves, the Samoan data show little variation in either $\alpha_{Sm/Nd}$ or ^{230}Th/^{238}U, this is consistent with them all being derived by similar extents of melting. However, on a more global scale when the Samoan data are considered in the context of the Hawaiian samples, which show a large range in composition (from tholeiites to basanites), they are remarkably consistent with the systematic relation between U-Th fractionation and Sm-Nd fractionation previously noted by *Sims et al.* [1995, 1999]. Sm/Nd is more fractionated than U/Th, and only samples that represent small melt fractions and have small $\alpha_{Sm/Nd}$ values show substantial U-Th fractionation, consistent with simple batch or accumulated fractional melting of a garnet lherzolite source, using a range of experimentally determined D_{Nd} and D_{Sm} [e.g., *McKay*, 1989; *Salters et al.*, 2002] and D_U and D_{Th} [*Beattie*, 1993a, 1993b; *Salters and Longhi*, 1999].

[40] U-Th and Sm-Nd data for the Samoan and Hawaiian samples can also be inverted in terms of batch melting models, to find self-consistent bulk U and Th partition coefficients and melt fractions. This inversion is based on the batch melting equation of *Shaw* [1970], which is linear when expressed in terms of the parameters $(1-\alpha_{Sm/Nd})^{-1}$ and $(1-(^{238}U/^{230}Th))^{-1}$ [*Sims et al.*, 1995]. For a given D_{Sm} and D_{Nd}, D_U and D_{Th} are uniquely determined and the melt fraction (F) can be calculated from the batch melting expression (see *Sims et al.* [1995] for details). For the Hawaiian and Samoan samples combined, regression of $(1-\alpha_{Sm/Nd})^{-1}$ versus $(1-(^{238}U/^{230}Th))^{-1}$ yields a slope of 13.0 ± 2.2 and an intercept of −24.8 ± 6.7, with an r^2 of 0.85. Assuming D_{Nd} = 0.02 and D_{Sm} = 0.04 [*Salters et al.*, 2002], we calculate D_U = 0.0038 and D_{Th} = 0.0021; these values are within the range of values calculated for a garnet lherzolite source using experimentally determined mineral/melt partitioning values for garnet and clinopyroxene (e.g. D_U = 0.0052 and D_{Th} = 0.0026 [*Salters and Longhi*, 1999]). Calculated melt fractions for Samoa are between 1.5–3%. For comparison, Hawaiian basalt melt fractions range from a maximum of 4–8% for tholeiites, to 0.5–2% for AOB, down to about 0.25% for basanites.

[41] Time-dependent melting models would shift all of the model curves upward in Figure 11a, as ingrowth of ^{230}Th would increase the ^{230}Th/^{238}U, but Sm/Nd fractionation would remain unchanged. The observation that there is a systematic relation between U-Th fractionation and Sm-Nd fractionation (Figure 11a), consistent with simple batch melting, implies that U-Th fractionation for Hawaiian and Samoan basalts is, in large part, a result of crystal-liquid fractionation occurring during partial melting in the presence of garnet. The

^{238}U-^{230}Th in Hawaii and Samoa are mainly sensitive to the small melt fractions because the upwelling rates for mantle plumes are fast relative to the long half-lives of ^{230}Th [*Elliott*, 1997; *Sims et al.*, 1995, 1999]. Many other data suites, particularly MORB, lie well above this simple batch-melting trend and require more complex melting models that incorporate ingrowth of daughter nuclides, multiple porosities and mixing of polybaric melts [cf. *Sims et al.*, 2002]. The influence of different source lithologies and respective productivities is also an important, but additional, parameter to consider [e.g., *Hirschmann and Stolper*, 1996].

6.1.2. ^{235}U–^{231}Pa

[42] ($^{231}Pa/^{235}U$) is greater than one in the four analyzed Samoan samples (Table 2). The relative values of ($^{230}Th/^{238}U$) and ($^{231}Pa/^{235}U$) for the Samoan lavas give an order of compatibility of $D_{Pa} < D_{Th} < D_U$, consistent with experimental and theoretical constraints [*Blundy and Wood*, 2003b].

[43] The ($^{230}Th/^{238}U$) – ($^{231}Pa/^{235}U$) of OIB, particularly Hawaii, define a near linear trend (Figure 12a) [*Pickett and Murrell*, 1997; *Sims et al.*, 1999; *Bourdon et al.*, 1998; *Bourdon and Sims*, 2003; *Lundstrom et al.*, 2003]. Although the Samoan data set is limited to only four samples, ($^{230}Th/^{238}U$) and ($^{231}Pa/^{235}U$) are coincident with this OIB array. This array, defined most distinctly by the Hawaiian data [*Sims et al.*, 1999], can be modeled by simple batch melting of a garnet peridotite, using experimentally determined partition coefficients for U and Th and assuming that Pa is highly incompatible (here we use $D_{Pa} = 10^{-5}$ to be consistent with *Bourdon and Sims* [2003] and *Sims et al.* [1999]) (Figure 12a).

[44] The Samoan basalts have small ^{230}Th and ^{231}Pa excesses that are comparable to Hawaiian shield-stage tholeiites from Mauna Loa and Kilauea and preshield stage tholeiites and alkali basalts from Loihi. Like ($^{230}Th/^{238}U$), ($^{231}Pa/^{235}U$) is also correlated with $\alpha_{Sm/Nd}$ (Figure 11b) and can thus be inverted in terms of batch melting models to find self-consistent bulk U and Pa partition coefficients and melt fractions. For the Hawaiian and Samoan samples combined, and assuming $D_{Nd} = 0.02$ and $D_{Sm} = 0.04$ [*Salters et al.*, 2002], we calculate $D_U = 0.004$ and $D_{Pa} = 0.00009$; these values are similar to those calculated (D_U) and inferred (D_{Pa}) for a garnet lherzolite source using experimentally determined D_U values for garnet and clinopyroxene [*Beattie*, 1993a, 1993b; *Blundy and Wood*, 2003a; *Salters and Longhi*, 1999]. Melt fractions for Samoa are between ~2–3% and, for Hawaiian basalts, range from a maximum of 8% for tholeiites, to 0.5–2% for AOB, down to about 0.25% for basanites. The simple systematic relationships between ($^{231}Pa/^{235}U$) – ($^{230}Th/^{238}U$) and ($^{231}Pa/^{235}U$) – Sm-Nd fractionation (Figures 11b and 12a) imply that U/Pa fractionation for Hawaiian and Samoan basalts is, in large part, a result of crystal-liquid fractionation occurring during partial melting in the presence of garnet. Similar to ($^{230}Th/^{238}U$), ($^{231}Pa/^{235}U$) in OIBs like Hawaii and Samoa is mainly sensitive to the small melt fractions because the upwelling rates for these mantle plumes are relatively fast compared to the long half-life of ^{231}Pa [*Elliott*, 1997; *Sims et al.*, 1995, 1999; *Bourdon and Sims*, 2003].

6.1.3. ^{230}Th–^{226}Ra

[45] In ten of the twelve Samoan samples, ($^{226}Ra/^{230}Th$) is greater than one and these ^{226}Ra excesses can be considered minimum values. However, for the four samples with ($^{210}Pb/^{226}Ra$) < 1, their eruption ages are interpreted be less than 100 years and their ^{226}Ra excess is considered unperturbed by posteruptive decay. When ($^{226}Ra/^{230}Th$) is compared with ($^{230}Th/^{238}U$) (Figures 4 and 13) and ($^{231}Pa/^{235}U$) (not shown), the relative extent of the disequilibrium gives an order of incompatibility of $D_{Pa} \approx D_{Ra} < D_{Th} < D_U$.

[46] The interpretation of ($^{226}Ra/^{230}Th$) in oceanic basalts is not straightforward. Large differences in Th and Ra crystal/liquid partitioning and the short-half life of ^{226}Ra can create large disequilibria during melting, particularly when ingrowth effects are considered [*McKenzie*, 1985; *Spiegelman and Elliot*, 1993; *Williams and Gill*, 1989]. In shallow magmatic systems, the relatively high partition coefficients for Ra in feldspars and amphiboles [*Blundy and Wood*, 2003a, 2003b] and its short half-life make it susceptible to secondary differentiation processes and/or timescales that can overprint its original melting signature [*Condomines et al.*, 2003; *Cooper et al.*, 2001, 2003; *Reagan et al.*, 1992; *Saal and Van Orman*, 2004].

[47] Despite a variety of interpretations for ($^{226}Ra/^{230}Th$) measured in oceanic basalts, it is generally agreed that simple time-independent melting models (i.e. batch or fractional melting) cannot explain the large ^{226}Ra excesses (Figure 12b). Because of its much shorter half-life, interpretation of ^{226}Ra data in terms of melting processes requires models that explicitly treat the time-scales of melt generation and melt extraction [e.g., *McKenzie*, 1985; *Spiegelman and Elliot*, 1993]. MORB data

seem to require more complicated 2-D melting scenarios (consistent with our understanding of the MORB melting regime), whereas simple 1-D time-dependent melting models can satisfactorily explain most OIB.

[48] Forward modeling shows that both 'chromatographic porous flow melting' [cf. *Spiegelman and Elliot*, 1993] and 'dynamic melting' [cf. *McKenzie*, 1985] of a garnet peridotite source can explain the $^{238}U-^{230}Th-^{226}Ra$ disequilibria in the Samoan samples. With chromatographic porous flow melting, the extent of ($^{230}Th/^{238}U$) disequilibrium is controlled mainly by the melting rate (related to the solid mantle upwelling rate) and ($^{226}Ra/^{230}Th$) disequilibrium is controlled mainly by the porosity of the melt region (which controls the velocity of the melt relative to the solid) (Figure 13a). Using an analytical approximation [*Sims et al.*, 1999] for the chromatographic porous flow model and the current experimental range of partition coefficients for U, Th and Ba (proxy for Ra) [*Beattie*, 1993a, 1993b; *La Tourrette and Burnett*, 1992; *La Tourrette et al.*, 1993; *Lundstrom et al.*, 1994; *Salters and Longhi*, 1999] the calculated maximum porosity in the melting zone ranges from 2%–6% and the melting rate ranges from 5E-3 to 2E-4 kg/m^3/yr. These inferred large maximum porosities, approach or exceed total melt fractions calculated from Sm-Nd fractionation implying no melt-solid movement during melting and thus no daughter nuclide ingrowth. With dynamic melting (not shown), ($^{230}Th/^{238}U$) disequilibrium is also controlled by the melting rate, however, the calculated porosities are threshold, or escape porosities. Because the dynamic melting model does not consider melt migration, for a given set of partition coefficients these threshold or escape porosities are considerably lower than the maximum porosities at the top of the melt column predicted by the chromatographic melting model. With dynamic melting, the inferred melting rates are also slightly lower. Finally, it is important to note that the Samoan ($^{231}Pa/^{235}U$) can also be explained by chromatographic porous flow melting (Figure 13b) and dynamic melting (not shown); these predict melting rates and porosities comparable to those obtained from $^{238}U-^{230}Th-^{226}Ra$.

[49] The above calculated melt fractions, porosities and melting rates, for both time-independent (batch and fractional) and time-dependent (chromatographic porous flow and dynamic) melting models, are highly dependent upon the absolute and relative values chosen for D_U, D_{Th}, D_{Pa} and D_{Ra} (Figures 12 and 13). Thus, until the effect of chemical composition, temperature and pressure on the measured partitioning values for U, Th, (and Pa and Ra) are established and the lithology of the mantle source is known explicitly, calculated solid mantle upwelling rates and porosities based upon ($^{230}Th/^{238}U$)($^{226}Ra/^{230}Th$) and ($^{231}Pa/^{235}U$) disequilibria must be considered as estimates only.

[50] Magma storage time is another potential source of uncertainty in the above modeling. If magma is stored in magma chambers for significant periods of time before eruption, the parent/daughter activity ratios will decay toward the equilibrium value and cause us to underestimate the parent/daughter fractionation in the melting process. This issue is most significant for ^{226}Ra; it is probably not a significant source of uncertainty for the longer-lived ^{230}Th and ^{231}Pa. While decay due to simple magma storage will reduce ^{226}Ra excesses, other effects such as plagioclase fractionation or cumulate-melt interaction during shallow level storage will also potentially affect ^{226}Ra excesses [*Reagan et al.*, 1992; *Sims et al.*, 1999; *Cooper et al.*, 2001, 2003; *Condomines et al.*, 2003; *Faul*, 2001; *Saal and Van Orman*, 2004]. Because ^{226}Ra in these models is largely controlled by the porosity of the melt zone, uncertainties in magma residence times will translate into large uncertainties in calculated porosities (i.e. Figure 13a), and the dominance of other Ra/Th fractionation mechanisms will negate the relevance of ^{226}Ra for determining melt porosities. Shallow level Ra/Th fractionation is not required but also it cannot be ruled out based on present data. However, as will be discussed below the moderate ^{210}Pb deficits seen in the Vailulu u' samples indicate short magma residence times relative to the half-life of ^{226}Ra. These samples isotopic heterogeneity over relatively short distances and time intervals also argues against substantial magma mixing and long magma storage times.

6.2. Implications for Mantle Upwelling Rates, Plume Structure, and Buoyancy Flux

[51] The calculated melting rates, determined mainly from U-Th and U-Pa disequilibria, can be combined with theoretical predictions of melt productivity [e.g., *McKenzie and Bickle*, 1988; *Asimow et al.*, 1997] to calculate solid mantle upwelling rates [*Sims et al.*, 1999; *Pietruszka et al.*, 2001; *Bourdon and Sims*, 2003; *Kokfelt et al.*, 2003; *Bourdon et al.*, 2006]. Using a theoretical melt productivity (dF/dz) of 0.003/km, which is an appropriate estimate for the depth range of interest

[*Asimow et al.*, 1997; *McKenzie and Bickle*, 1988], we calculate solid mantle upwelling rates from ~2 cm/year to ~50 cm/year for Samoan magma generation. These upwelling rates are reasonable, but quite variable, ranging from the lower end of upwelling rates calculated (from U-series data) for Hawaiian main-stage tholeiites (40–100 cm/year) down to values typical for Hawaiian postshield alkali basalts (2–5 cm/year). Previous studies of OIB have shown a positive correlation between (^{230}Th/^{238}U) and distance from a plume center, and this has universally been attributed to variations in upwelling rate [*Sims et al.*, 1999; *Pietruszka et al.*, 2001; *Bourdon and Sims*, 2003; *Kokfelt et al.*, 2003; *Bourdon et al.*, 2006]. In this regard, it is important to note that for Hawaiian basalts, upwelling rates inferred from U-series data [*Sims et al.*, 1999; *Pietruszka et al.*, 2001] are comparable to upwelling velocities calculated from axis-symmetric plume models [*Watson and McKenzie*, 1991; *Hauri et al.*, 1994] and are even better matched [*Bourdon and Sims*, 2003] with models that take into account the influence of the overriding Pacific plate on plume upwelling [*Ribe and Christensen*, 1999]. *Chabaux et al.* [1994] first noted a rough negative correlation between U-series disequilibria and plume buoyancy flux, and this has been since modeled as function of "coupled variations in excess mantle temperature and upwelling velocity" [*Bourdon et al.*, 2006]. The Samoan data presented here generally conform to these correlations, but the ^{230}Th and ^{231}Pa excesses are low for its estimated buoyancy flux [*Ribe*, 1996; *Sleep*, 1990]; at face value, this would change the functional form of this correlation, making it more hyberbolic than previously estimated [*Bourdon et al.*, 2006] and inferring higher temperature anomalies in the plume-generating boundary layer. Alternatively, the buoyancy flux for Samoa may be significantly underestimated, as Samoa sits adjacent to a complicated tectonic regime (Tonga subduction).

7. Implications of ^{210}Pb Disequilibria for Continuous Magma Degassing

[52] While most of the Samoan samples are in equilibrium with respect to (^{210}Pb/^{226}Ra) and are thus interpreted to be older than 100 years, three of the Vailulu'u crater samples show significant (^{210}Pb/^{226}Ra) disequilibria with ^{210}Pb deficits of ~30%. While the ages of two of these samples (73-3; 63-13) are uncertain relative to the half-life of ^{210}Pb, the ALIA 101 sample's age is known to be recent (November 2004) and so its ^{210}Pb deficit can be considered unperturbed by posteruptive decay.

[53] The interpretation of (^{210}Pb/^{226}Ra) disequilibria is even more uncertain than (^{226}Ra/^{230}Th), as a number of mechanisms can potentially fractionate (^{210}Pb/^{226}Ra) including: partial melting; sulfide fractionation; plagioclase crystallization; and magma degassing. While Pb is only slightly volatile (its measured gas/melt emanation coefficient is only ~0.0015 [*Lambert et al.*, 1985; *Rubin*, 1997]), sustained continuous degassing of intermediate daughter ^{222}Rn can create large ^{210}Pb deficits in magmas [*Gauthier and Condomines*, 1999; *Rubin and Macdougall*, 1989; *Sims and Gauthier*, 2007].

[54] Most (^{210}Pb/^{226}Ra) measurements have been on subaerial volcanic arc samples [e.g., *Berlo et al.*, 2006; *Gauthier and Condomines*, 1999; *Reagan et al.*, 2006; *Turner et al.*, 2004], though a few measurements have been reported for submarine samples from Macdonald seamount [*Rubin and Macdougall*, 1989] and Pacific MORB [*Rubin et al.*, 2005]. The large ^{210}Pb deficits seen in the Macdonald seamount basalts, and for many arcs, have been interpreted in terms of Rn degassing, plus or minus some plagioclase fractionation [*Gauthier and Condomines*, 1999]. In contrast, the (^{210}Pb/^{226}Ra) disequilibria in samples from historic MORB eruptions are quite small (0.9–1.1) and have been attributed to melt generation processes and short magma transport/residence times [*Rubin et al.*, 2005].

[55] As was proposed for MORB [*Rubin et al.*, 2005], melt generation processes can also explain the large ^{210}Pb deficits measured at Vailulu'u. The much greater compatibility of Pb relative to Ra can create significant ^{210}Pb deficits using both time-dependent and time-independent melting models. For example, using D_{Pb} of 0.021 (for a garnet peridotite using compiled mineral D's from *Hart and Gaetani* [2006]) and D_{Ra} of 4E-5, a (^{210}Pb/^{226}Ra) of 0.75 can be produced by ~0.6% simple batch melting. Pb is also highly chalcophilic, so that residual sulfide during melting would make Pb even more compatible [*Sims and DePaolo*, 1997; *Hart and Gaetani*, 2006]. Also, sulfides frequently appear as liquidus phases in Vailulu'u magmas [*Workman et al.*, 2006], thus differentiation processes would also cause ^{210}Pb deficits. For example, if the sulfide/melt partition coefficient is 38 [*Hart and Gaetani*, 2006], and Ra is considered to be 100% incompatible in sulfides, then ~0.9% sulfide crystallization is required to produce a ^{210}Pb deficit of 25%. However, there is not enough

S in estimated primary Samoan melts to allow for more than 0.1–0.2% sulfide crystallization [*Workman et al.*, 2006].

[56] Furthermore, the S/Cl ratio in Samoan glasses is relatively constant, again arguing against significant sulfide fractionation [*Workman et al.*, 2006]. However, in all cases, if the large ^{210}Pb deficits observed in Vailulu'u are a result of magmatic processes (melting or differentiation), then extremely short magma residence times are inferred (ca. 20 years or much less).

[57] Continuous ^{222}Rn degassing [*Gauthier and Condomines*, 1999; *Rubin and Macdougall*, 1989; *Turner et al.*, 2004; *Sims and Gauthier*, 2007] can also explain the large ^{210}Pb deficits measured at Vailulu'u. This hypothesis is consistent with the large extent of ^{210}Po degassing measured for ALIA 101-01 and the very high hydrothermal ^{3}He contents observed in water from Vailulu'u crater [*Staudigel et al.*, 2004]. Efficient degassing of radon at shallow magma levels is also supported by measurements of low initial ^{222}Rn and ^{210}Po in freshly erupted mafic and intermediate lavas [*Gill et al.*, 1985; *Sato*, 2003; *Sato and Sato*, 1977; *Reagan et al.*, 2008], and by measurements of high (^{222}Rn/^{210}Pb) in volcanic gases coming directly from dry magma conduits, such as Masaya [*Sims and Gauthier*, 2007]. For the ^{210}Pb deficit measured for the zero-age sample ALIA 101-01 (0.70), and using a variety of degassing models (with or without magma recharge, and with partial or complete degassing [*Gauthier and Condomines*, 1999]), inferred residence times are short (~10–30 years), consistent with the observation that there have been numerous isotopically distinct lava eruptions within the Vailulu'u summit crater over the past 100 years. Because ^{222}Rn degases by partitioning into a vapor phase created by the major volatile species (e.g. H_2O and CO_2 [*Gauthier and Condomines*, 1999]), these models imply that Samoan magmas persistently exsolve H_2O and CO_2 [*Workman et al.*, 2006] for decadal time frames before eruption.

8. Conclusions

8.1. With Regard to Sample Eruption Ages

[58] 1. For the submarine volcano Vailulu'u, (^{230}Th/^{238}U) and (^{226}Ra/^{230}Th) disequilibria indicate that all of the samples from the summit crater and lower rift zones have maximum eruption ages of <350 ka, with most being <8 ka. These young eruption ages imply that Vailulu'u is magmatically productive, consistent with the hypothesis that it is at the leading edge of the Samoan plume [*Hart et al.*, 2000, 2004].

[59] 2. Geological observations [*Hart et al.*, 2000, 2004; *Staudigel et al.*, 2004] and (^{210}Pb/^{226}Ra) and (^{210}Po/^{210}Pb) disequilibria indicate that Vailulu'u has been recently active, with several lava-producing eruptions within the summit crater over the past 100 years.

[60] 3. For the newly-mapped Nafanua volcanic cone, the ^{210}Po ingrowth age indicates an eruption date of Nov 08, 2004 (+62/−67 days). This age is consistent with observational cruise data that place its eruption date between March 1999 and April 2005.

[61] 4. For submarine volcano Malumalu (^{230}Th/^{238}U), (^{231}Pa/^{235}U) and (^{226}Ra/^{230}Th) indicate that there are at least three flows with maximum eruption ages of <350 ka. One of these flows also has ^{231}Pa excess and is inferred to be less than 150 Ka; another (78-1) has ^{226}Ra excess and is inferred to be <8 ka.

[62] 5. The young coeval volcanism on Malumalu and Vailulu'u suggests that the Samoa hot spot is currently feeding both volcanoes, though they lie on separate volcanic lineaments. This may indicate a northeast migration of the Samoa plume due to dynamic interaction with the Tonga slab.

8.2. With Regard to Samoan Basalt Petrogenesis

[63] 1. (^{230}Th/^{232}Th) and (^{238}U/^{232}Th) of the Samoan lavas are variable and well-correlated with long-lived radiogenic isotopes (e.g. ^{87}Sr/^{86}Sr, ^{143}Nd/^{144}Nd and ^{208}Pb/^{206}Pb) and incompatible trace element ratios (e.g. La/Yb). These correlations suggest that the enriched Th/U ratio of the Samoan source is a long-lived feature and that source variability is exerting a primary influence on trace element abundances in these basalts.

[64] 2. (^{230}Th/^{238}U) in the Samoan lavas are limited in range and extent and show no systematic variation with either long-term source characteristics (e.g. ^{87}Sr/^{86}Sr; ^{143}Nd/^{144}Nd, ^{206}Pb/^{204}Pb) or trace element ratios and abundances (e.g. La/Yb). However, the lavas are all alkaline basalts derived by similar extents of mantle melting, so trace element variations induced by differences in degree of melting are small compared to the large variability inherited from the source.

[65] 3. The (^{230}Th/^{238}U) and (^{231}Pa/^{235}U) disequilibria in these Samoan basalts, because of the relatively long half-lives of ^{230}Th and ^{231}Pa, can

be modeled in terms of batch melting. This suggests that a significant portion of the (^{230}Th/^{238}U) and (^{231}Pa/^{235}U) disequilibria result from net U/Th and U/Pa elemental fractionations during melting.

[66] 4. The (^{226}Ra/^{230}Th) disequilibria require time-dependent or "ingrowth" models that treat explicitly the time scales of melt generation and melt extraction. The combined (^{230}Th/^{238}U), (^{226}Ra/^{230}Th) and (^{231}Pa/^{235}U) disequilibria can be understood in terms of variations in the melting parameters porosity and melting rate (related to solid mantle upwelling rate).

[67] 5. Four Vailulu'u summit crater samples show significant ^{210}Pb deficits relative to ^{226}Ra. These ^{210}Pb deficits are interpreted in terms of a model of continuous degassing of ^{222}Rn and infer magma residence times in the shallow crust of l0–30 years. The inference that these Vailulu'u samples have undergone short decadal scale magma storage times is supported by two other observations: the first is that the Vailulu'u summit crater samples show significant isotopic heterogeneity over relatively short distances and time intervals arguing against substantial magma mixing and long magma storage times; the second is that ALIA 101-01 had (^{228}Ra/^{232}Th) in equilibrium at the time of eruption suggesting a magma residence/transport time of no less than 10–15 years.

Appendix A: Analytical Methods

A1. WHOI Mass Spectrometry Methods for U and Th Isotopes and ^{238}U, ^{232}Th, ^{226}Ra, and ^{231}Pa Concentrations

A1.1. Sample Preparation

[68] Approximately 0.5 to 2.0 grams of 1–5 mm size ocean floor basalt glasses are carefully hand–picked, and then ultrasonicated in sequential batches of distilled acetone, 18 M ohm H_2O, 0.1 M high purity oxalic acid + 2% high purity H_2O_2, 0.1 M seastar HCl + 2% H_2O_2, 18 M ohm H_2O and distilled high purity acetone. After drying thoroughly the sample is then carefully hand-picked one additional time. Careful hand-picking and light leaching has been shown to be crucial to eliminate contamination associated with Mn oxides and ocean sediment [*Bourdon et al.*, 2000; *Sims et al.*, 2001, 2002]. Note that such leaching has been shown in experiments using subaerial rock standards (e.g. TML and ATHO) not to perturb the samples U/Th, Th/Ra and U/Pa [*Bourdon et al.*, 2000; *Sims et al.*, 2002].

A1.2. Sample Dissolution

[69] After leaching and crushing (1–5 mm) the terrestrial rock samples and ocean floor basalt glasses are dissolved completely by a series of digestions using HF and HNO_3, followed by HNO_3+H_3BO_3 and $HCLO_4$ to break down all fluorides. During these steps it is essential to attain complete digestion and eliminate all fluorides as incomplete dissolution and residual fluorides will reduce column yields and perturb the sample's U/Th, U/Pa and Th/Ra.

A1.3. Thorium and Uranium Isotopes

[70] From the dissolved rock samples thorium and uranium separated and purified in the WHOI clean labs using two anion columns. The first column is a nitric anion column to separate Th and U from the silicate rock matrix, and the second column is a hydrochloric anion column to separate Th from U.

[71] Th isotopes are measured using the WHOI ThermoFisher NEPTUNE. Analyses are made statically, measuring ^{232}Th on a Faraday cup and ^{230}Th on the axial, discrete dynode ion counter (ETP-SEM/SGE, Sydney, Australia) passing through a tunable repelling potential quadrupole (RPQ) or high abundance sensitivity lens designed to minimize tailing on the low mass side of a peak. Using the RPQ on the ThermoFisher Neptune, the abundance sensitivity at 85% transmission was ~50 ppb over 2 AMU, resulting in a tail correction of ^{232}Th on ^{230}Th of 0.7% for ^{230}Th/^{232}Th of 3.3×10^{-6} and 0.3% for ^{230}Th/^{232}Th of 6.7×10^{-6}. For each sample and standard the tailing of ^{232}Th on ^{230}Th is corrected offline using an exponential method, based on a peak scan from mass 229.5 to mass 231.5. These scans show tail curvature on the NEPTUNE is such that a linear extrapolation would significantly overestimate the effect of the ^{232}Th tailing, thereby causing the corrected ^{230}Th/^{232}Th ratio to be too low. To correct for both instrumental mass fractionation between masses 230 and 232 and the relative difference in the efficiency of the Faraday and SEM detectors, we evaluated two different methodologies: (1) a linear interpolation of the ^{238}U/^{236}U measured in NBS U010 interspersed between each sample and normalized to its certified value (14,535 ± 149), and (2) a linear interpolation of the ^{230}Th/^{232}Th measured in the UCSC Th 'A' interspersed between each sample, and normalized to its nominal value

5.856×10^{-6} (± 1.2% 2s RSD) from *Rubin* (2001). Results show that, due to instrumental mass bias differences and differences of the ion energies through the RPQ filter of U and Th, U does not adequately correct for Th and generally gives results that are too low [*Ball et al.*, 2008; *Sims et al.*, 2008]. Thus for this study and all Th isotopic analyses at WHOI, Th isotopic measurements are corrected using a linear interpolation of the $^{230}Th/^{232}Th$ measured in the UCSC Th 'A' bracketing each sample, and normalized to a nominal value from *Rubin* (2001). Sensitivity, based on U using a normal spray chamber (wet plasma) and standard nickel cones, expressed as ion yield is approximately 0.1%. The linear range of the ETP SEM with RPQ is less than 20k CPS, with the best linearity achieved by matching samples and standards to within a factor of 2. Dead time was measured to be 20 nanoseconds. Using Th-bracketing (UCSC Th 'A'), interday reproducibility over a four-year period with multiple instrument operators is 0.4–1.5% (2s) for both solution standards and processed Th from volcanic samples. Our daily reproducibility for any one solution is 0.2–0.5% (2s). Drift in UCSC Th 'A' varies from 0.5 to 1.0% throughout a 10-hour analytical session after a 2–3 hour warm-up period. Temporal variations in drift and abundance sensitivity throughout each session are the most fundamental sources of error.

[72] U isotopes are measured using the WHOI ThermoFisher NEPTUNE. We measure ^{238}U and ^{235}U on Faraday collectors and ^{234}U (or ^{236}U) on the SEM. $^{236}U/^{238}U$ ratios are measured in the synthetic uranium standard U010 (New Brunswick Laboratory, New Brunswick, IL) to calibrate the SEM yield or efficiency and correct for mass bias drift. Time dependent drift correction of both SEM yield and instrumental mass bias are required to produce accurate, reliable data. The suite of uranium standards offered by the New Brunswick Lab such as U010 are well characterized and useful as a calibration standards for uranium measurements. Because of the higher abundances of the minor uranium isotopes, the requirements for ion counting uranium isotopes are not as demanding with regard to abundance sensitivity as those for thorium isotopes. With the RPQ turned off, the tail of ^{238}U on ^{234}U is 4ppb and the tailing of ^{235}U on ^{234}U is 5ppm, making the tail correction for ^{238}U and ^{235}U on ^{234}U small relative to other uncertainties and thus unnecessary. Comparison of $^{234}U/^{238}U$ measurements made with the RPQ set to 85% transmission show precisions a factor of two larger than with the RPQ shorted to ground. The degradation of measurement precision with the RPQ on is about one per mil based on 10 measurements each of NBL112A with and without RPQ. Standard-sample-standard bracketing for uranium analysis allows correction for SEM calibration and drift. We find that optimum accuracy is obtained by using ^{234}U in U010 as a yield monitor of SEM efficiency when measuring ^{234}U in unknown samples. We have the option of monitoring instrumental fractionation either with the same ratio and combining the yield and mass bias correction into one factor or by tracking the mass bias drift with the $^{235}U/^{238}U$ ratio (approximately 0.01 in U010) on Faraday collectors. We have detected no difference in data quality between the two methods principally because the SEM yield determination is error limiting. Further details of these methods and replicate analyses of synthetic and rock standards are given by *Ball et al.* [2008] and *Sims et al.* [2008].

A1.4. ^{238}U and ^{232}Th Concentrations

[73] Uranium and thorium concentrations on separate liquid aliquots from the same rock dissolution are determined by isotope dilution using the ThermoFisher Element 2 high resolution sector-field ICPMS. Rock sample aliquot sizes are estimated so as to contain ~10 ng of ^{238}U. Each aliquot is spiked with individual ^{229}Th and ^{233}U spikes and equilibrated, using progressive dry downs and perchloric acid fuming. Samples are spiked to attain $^{232}Th/^{229}Th \approx 30$ and $^{238}U/^{233}U \approx 10$. A nitric anion column is used to separate Th and U from most of the silicate matrix. ^{229}Th and ^{233}U are calibrated against gravimetric solutions of ^{238}U (made from NBS 960 metal) and ^{232}Th (made from Ames metal) and are known to better than 1% (2s).

[74] U and Th are measured in the same aliquot using a peak hopping routine on masses 229, 232, 232.5, 233, 235, 238. The most abundant isotope (typically ^{232}Th) is kept below 5 million counts per second so that all measurements are made in pulse counting mode. Mass 232.5 is monitored to assess tailing of mass 232 onto mass 233 and vice versa; mass 234 is monitored to assess tailing of mass 235 onto mass 233 and vice versa. Prior to each analysis a scan of the spectra from mass 226 to mass 240 is conducted to evaluate background. Because the $^{235}U/^{238}U$ of the spike is un-natural, instrumental mass fractionation is corrected by sample/standard bracketing using a linear interpolation of the $^{235}U/^{238}U$ measured in NBL-112A interspersed between each sample. Samples are run in triplicate and so each analysis and its uncertainty

represent the average and 2 sigma standard deviation of these triplicate analyses.

A1.5. ^{226}Ra Concentrations

[75] ^{226}Ra concentrations on separate liquid aliquots from the same rock dissolution are determined by isotope dilution using the ThermoFisher Neptune at WHOI. Rock sample aliquot sizes are estimated so as to contain ~30–100 fg of ^{226}Ra. Each aliquot is spiked with ^{228}Ra. and equilibrated, using progressive dry downs and perchloric acid fuming. Samples are spiked to attain ^{226}Ra/^{228}Ra ≈ 10.

[76] WHOI's ^{228}Ra spike is 'milked' from NIST SRM 3159 (lot No. 992912) 9.8 mg/g Th standard and calibrated against NIST 4967 ^{226}Ra std, which has an overall uncertainty on its certified ^{226}Ra concentration of 1.18% (NIST Certificate-https://srmors.nist.gov/certificates/view_cert2gif.cfm?certificate=4967).

[77] After spiking and spike equilibration Ra purification was accomplished using slightly modified procedures from [*Chabaux et al.*, 1994]. Briefly, the Ra fraction is separated from U and Th on a large (8–10 ml) HNO_3 anion column (AG1X8 200–400 mesh). Ra is then purified using a series of HCl elutions on a large (8–10 ml) cation column (AG50 X8 cation resin). Ra is further purified with another pass through a 2 ml column of AG 50 X8 resin Ra-Ba separation was accomplished with two passes through a 500 ml column of Sr-spec resin eluting with 3N HNO_3. Immediately prior to mass spectrometry ^{228}Ra is separated from the ingrown ^{228}Th using a small HCl cation column. All samples are also fumed prior to mass spectrometry to reduce organic backgrounds and intereferences.

[78] Using ^{228}Ra as an isotope spike we have investigated two ion-counting methods; a "peak-hopping" routine, where ^{226}Ra and ^{228}Ra are measured in sequence on the central discrete dynode ETP secondary electron multiplier (SEM), and simultaneous measurement of ^{226}Ra and ^{228}Ra on two multiple ion-counter system (MICS) channeltron type detectors mounted on the low end of the collector block. Here we present ^{226}Ra measurement by isotope dilution using the Thermo Fisher NEPTUNE MC-ICPMS. Analysis of external rock standards TML and ATHO along with mid-ocean ridge basalt (MORB) and ocean island basalt (OIB) samples show three issues that need to be considered when making precise and accurate Ra measurements: (1) mass bias, (2) background, and (3) relative efficiencies of the detectors when measuring in MIC mode.

[79] Due to the absence of an established ^{226}Ra/^{228}Ra standard, we have used U reference material NBL-112A to monitor mass bias. Although *Ball et al.* [2008] have shown that U does not serve as an adequate proxy for Th (and thus not likely for Ra either), measurements of rock standards TML and ATHO are repeatedly in equilibrium within the uncertainty of the measurements (where total uncertainty includes propagation of the uncertainty in the ^{226}Ra standard used for calibrating the ^{228}Ra spike). For this application, U is an adequate proxy for Ra mass bias at the 1% uncertainly level. The more important issue is the background correction. Because of the extensive chemistry required to separate and purify Ra (typically fg/g level in volcanic rocks), we observe large ambient backgrounds using both ion-counting techniques, which can significantly influence the measured ^{226}Ra/^{228}Ra ratio. Ra off-peak backgrounds need to be measured explicitly and quantitatively corrected for. One advantage of using a "peak-hopping" routine on the central SEM is the optional use of the high abundance sensitivity lens or repelling potential quadrapole (RPQ). This lens virtually eliminates the ambient background and significantly enhances the signal to noise ratio with only a small decrease in Ra ion transmission. Even with the diminished background levels observed using "peak-hopping" on the SEM with the RPQ, accurate measurement of Ra isotopes requires off-peak background measurement. Finally, when using MICS it is important to account for the relative efficiency of the detectors. Multiple ion counting is, in principle, preferable to "peak-hopping" because more time is spent counting each individual isotope. However, our results illustrate that proper calibration of detector yields requires dynamic switching of ^{226}Ra between the two ion counters. This negates the inherent advantage of multiple ion counting. Therefore, when considering mass bias, background correction, and detector gain calibration, we conclude that "peak-hopping" on the central SEM with the RPQ abundance filter is the preferred technique for ^{226}Ra/^{228}Ra isotopic measurement on the Neptune MC-ICPMS. The Samoan samples analyzed for this study were measured using a "peak-hopping" routine on the central SEM and the RPQ abundance filter.

A1.6. ^{231}Pa Concentrations

[80] ^{231}Pa is measured using the WHOI ThermoFisher ELEMENT2 using techniques previously

published in *Choi et al.*, 2001 and *Pichat et al.*, 2004. The reader is referred to these paper for a more detailed description of the analytical protocols used at WHOI. Although these papers are written with an emphasis on the analysis of ocean waters and sediments, high-precision measurements of ^{231}Pa have also been obtained on volcanic samples (MORB, OIB and IA lavas) using this technique. In fact, this technique uses Table Moutain Lattite (TML) as an equilibrium standard for calibrating the ^{231}Pa spike. In the following we provide a brief overview of the ^{231}Pa protocol at WHOI.

[81] From the dissolved sample solutions described above an aliquot of sample is separated and spiked to have ^{233}Pa (0.5–2 pg) and = ^{231}Pa/^{233}Pa ratios of 1–5. This spike liquid sample aligout mixture is then refluxed with $HClO_4$ to equilibrate spike and sample, and to further destroy fluoride complexes, which could decrease Pa recovery during separation and purification. In the course of the evaporation, 8N HNO_3 was used repeatedly to wash beaker walls (~6 ml total). The sample is evaporated to near dryness and 20 ml of 2N HCl was added to bring the spiked sample back into solution. 10 ml of concentrated NH_4OH were added to this ^{231}Pa aliquot to precipitate iron oxyhydroxides (pH = 8–9) entrain Pa. The Fe concentrations of volcanic samples are high enough to avoid using a Fe-carrier as is required for seawater [e.g., *Choi et al.*, 2001]. Avoiding the use of a Fe-carrier reduces the procedural blanks. Fluoride ions remained in solution, thus avoiding formation of stable fluoride complexes (PaF_7^{2-}), which would compromise the efficiency of the following Pa elution. This Fe oxyhydroxide precipitate is cleaned by successive dissolution with Milli-Q water and 2N HCl and then reprecipitated with NH_4OH (pH = 8–9). Between each step the sample was centrifuged and the supernatant was discarded. Finally, the precipitate was dissolved in 9N HCl. The iron precipitation step is important as both an initial purification step and a means of removing fluoride ions. Pa is then separated and purified by three successive 4ml anion exchange columns (AG1 × 8, 100–200 mesh) using a procedure modified from the methods described by *Anderson and Fleer* [1982] and *Fleer and Bacon* [1991]. See *Choi et al.* [2001] for details. γ-counting experiments showed a final recovery of 98% ± 8% ^{233}Pa.

[82] ^{231}Pa concentrations were determined by isotope dilution (see below for discussion of spike preparation and calibration). Measurements were made with ThermoFisher ELEMENT2 ICPMS in low-resolution mode (mass resolving power Δm/m = 300). Samples were introduced into the plasma through a membrane desolvation system (MCN-6000, Cetac Technologies) equipped with a PFA microconcentric nebulizer and a redesigned PFA spray chamber (Elemental Scientific Inc.) heated at 100°C. The redesigned chamber improved plasma stability by more efficiently removing wet droplets which could have passed through the plasma. Passive aspiration was used to improve the stability of the ion beam and eliminate possible memory effects from the PVC tubes of a peristaltic pump. Combining the MCN-6000 and PFA microconcentric nebulizer significantly reduces the sample uptake rate to <80 μl/min and improves sensitivity to 5–8 × 10^6 cps/ppb U (i.e. a factor of 5 to 10) compared to standard pneumatic nebulization without desolvation, without increasing background counts. The resulting overall efficiency is 1.5 to 2.5‰ (ions detected/atoms introduced) for U. Measurements were made in the electrostatic scanning mode by changing the acceleration voltage with a fixed magnetic field. Data acquisition time was 2–3 minutes for each fraction. The acquisition of all the data (^{231}Pa, ^{230}Th, ^{232}Th and ^{238}U concentrations) necessary for 18 samples and 2 procedural blanks can be made within 48 hours. The instrumental mass fractionation was evaluated by bracketing each unknown sample with a uranium standard (see section 3.6). For this purpose, we used the ^{235}U/^{238}U of National Bureau of Standards NBS 960.

[83] The ^{233}Pa spike was produced by neutron activation of ^{232}Th and was purified by anion AG1-X8 resin [*Anderson and Fleer*, 1982]. The ^{233}Pa solution was calibrated by ThermoFisher ELEMENT2 ICPMS with the ^{231}Pa of a TML solution, which has (^{231}Pa/^{235}U) of unity. However, since TML is not homogeneous with respect to U and Th, the ^{231}Pa concentration in TML was calculated on the basis of the ^{235}U-^{231}Pa secular equilibrium, using the ^{235}U concentration determined by ThermoFisher ELEMENT2 ICPMS against a ^{236}U spike. The external errors for these measurements are <2.2% (2σ SD). Also, after the ^{233}Pa spike had decayed for more than seven half-lives (i.e. more than 4 months), the number of ^{233}Pa atoms is essentially zero and all the atoms at mass 233 are ^{233}U. Since U and Pa were efficiently separated when the spike was purified after six months, the ^{233}U atom concentration is equal to the initial ^{233}Pa atom concentration of the spike enabling us to determine the ^{233}Pa concentration by

measuring ^{233}U in the spike against a calibrated ^{236}U spike. The results of these measurements typically agree with the ^{233}Pa calibration made against the TML rock standard (Table 3a) to within less than 2.5%, i.e. close to the external error of the calibration of the ^{233}Pa made against TML.

A2. WHOI Gamma Spectrometry Methods for Short-Lived U and Th Decay Series Nuclides

[84] Activities of several short-lived isotopes were measured by gamma spectrometry [*Condomines et al.*, 1987]. Approximately 10 gm of rock powder (grain size <100 mm) was poured into plastic vials. Each sample vial was inserted into a closed-end coaxial well-type High Purity Germanium (HP-Ge) detector manufactured by CANBERRA that is assembled inside a protective lead and copper shield.

[85] The resolution of this low-energy HP-Ge detector is <3.0 keV at 1.33 MeV and <2.0 keV at 122 keV with ~40% relative efficiency. The outer diameter and length of the detector are 65mm each while the diameter and depth of the well are 33 mm and 48 mm, respectively. The well-type detector geometry provides high efficiency for small samples because the sample is virtually surrounded by active detector material on all sides except the top. Germanium detectors are cooled with liquid nitrogen, which has a temperature of 77 K, to prevent thermal generation of charge carriers as well as to protect the detector surfaces from moisture and other contaminants.

[86] Cosmic radiation, mostly muons and neutrons, are the main contributors to germanium detector's background [*Heusser*, 1995]. The cosmic radiation interacts with the lead shielding to produce the spectral baseline seen in the germanium gamma spectrum. This Canberra detector uses a single large fast plastic scintillation shield (80 cm × 80 cm × 5 cm, Bicron BC408 Newbury, Ohio, www.bicron.com) above the gamma detector. The signal from the fast plastic scintillator must be delayed to match the signal from the germanium crystal. Then an appropriate timing window must be experimentally determined which is long enough to veto the errant signal but not so long as to increase the dead time of the detector. An approximate improvement (reduction of background) of 35% is shown between 30–1200 keV with no noticeable increase in dead time.

[87] In an effort to reduce the Radon daughter background component from the ambient lab air, the detector operates with a Plexiglas glove box enclosure around the lead shielding in a positive pressure nitrogen atmosphere. It has airtight side chambers to introduce and remove samples without opening the whole system to ambient air. The 2 liters of LN_2 which boil off from the dewar produces more than 1400 Liters of pure nitrogen gas daily. This nitrogen gas is captured at the top of the dewar and ducted into the Plexiglas box. There are two gloves for manipulating the shield door, changing samples and moving racks of samples in and out of the antechambers. With the use of a N_2 radon reduction box, a small but noticeable reduction in the background is observed.

[88] The HP-Ge detector can measure gamma rays in the approximate range of 40–11,000 keV although the efficiency of the detector is linear only up to ~100 keV. For higher energy gamma rays, a correction is applied for detector sensitivity. For our study, gamma rays in the range of 40–950 keV were measured. A self-absorption correction, taking into account differences in density and chemical compositions of the rock powders is also routinely applied. This correction is only significant for the low-energy gamma rays, such as the 46.5 keV peak of ^{210}Pb (maximum 20%). For the other peaks of interest above 300 keV, the self-absorption correction is negligible.

[89] The activity of ^{226}Ra is determined through four different gamma rays: 186.0 keV of ^{226}Ra, 295.22 and 351.99 keV lines of ^{214}Pb and the 609.32 keV line of ^{214}Bi. However, because of interferences and large uncertainties with 186.0 keV of ^{226}Ra, and 295.22 keV lines of ^{214}Pb, we only report the 351.99 keV lines of ^{214}Pb and the 609.32 keV line of ^{214}Bi.

[90] The activity of ^{232}Th is determined through three different gamma lines: 338.4 keV and 911.07 keV of ^{228}Ac, and 583.14 of ^{208}Tl. The 911.07 keV is preferred for ^{228}Ac and used here.

[91] The activities of the different nuclides are calculated by comparing the count rates (counts per hour per gram of sample) of a given peak for the sample and standard. For a calibrating standard, of similar density and composition, we use ATHO and assume all its daughter nuclides from ^{230}Th on down to ^{206}Pb and ^{232}Th on down to ^{208}Pb are in secular equilibrium. This is reasonable as numerous mass spectrometric analyses of ^{226}Ra/^{230}Th show it to be in equilibrium. For quality assurance we have also measure USGS standards BCR2 and W2 as unknowns. These standards are also in

equilibrium, and as such provide an important measure of accuracy.

A3. University of Iowa Alpha Spectrometry Methods for ^{210}Po Measurements

[92] Analytical techniques for ^{210}Po are discussed in detail elsewhere [*Reagan et al.*, 2005]. Briefly, ^{209}Po spike solution calibrated against a (^{210}Po) value of 7.95 dpm/g for TML (Table Mountain Latite) was added to ~2 grams of sample. The samples were then digested in a 2:1 mixture of concentrated HF and HNO_3 and brought into solution in 1 N HCl with a small amount of boric acid. This solution was run through a single anion exchange column to assure clean plating. Yields through chemistry generally exceed 90%. Po is autoplated on Ag disks in 150 ml of warm 0.5 N HCl with about 20 mg of ascorbic acid solute for 8–10 hours. Samples were counted on an alpha spectrometer for about one week. For the ALIA 101-01 whole rock initial (^{210}Po) and (^{210}Pb) values and errors for samples were calculated by exponential regressions through three analyses of single whole-rock powders employing a half-life for ^{210}Po of 138.4 days [*Holden*, 1990]. For the rest of the samples, (^{210}Pb) was considered to equal (^{210}Po).

Acknowledgments

[93] Constructive comments by Vincent Salters, Tim Elliott, Mary Reid and an anonymous reviewer are gratefully appreciated. Editorial handling by Vincent Salters is also acknowledged. Support for this research was provided by NSF grants EAR-9909473 (KWWS), EAR-0509891 (SRH), EAR-0609670 (MKR) and EAR-0504362 (MKR).

References

Anderson, R. F., and A. P. Fleer (1982), Determination of natural actinides and plutonium in marine particulate matter, *Anal. Chem.*, *54*, 1142–1147.

Asimow, P. D., M. M. Hirschmann, and E. M. Stolper (1997), An analysis of variations in isentropic melt productivity, *Philos. Trans. R. Soc. London*, *355*, 255–281.

Ball, L. A., K. W. W. Sims, and J. Schwieters (2008), Measurement of ^{234}U/^{238}U and ^{230}Th/^{232}Th in volcanic rocks using the Neptune PIMMS, *J. Anal. Atomic Spectrometry*, *23*, 173–180, doi:10.1039/b703193a.

Beattie, P. (1993a), The generation of uranium series disequilibria by partial melting of spinel peridotite: Constraints from partitioning studies, *Earth Planet. Sci. Lett.*, *117*, 379–391.

Beattie, P. (1993b), Uranium-thorium disequilibria and partitioning on melting of garnet peridotite, *Nature*, *363*, 63–65.

Bennett, J. T., S. Krishnaswami, K. K. Turekian, W. G. Melson, and C. A. Hopson (1982), The uranium and thorium decay series nuclides in Mt. St. Helens effusives, *Earth Planet. Sci. Lett.*, *60*, 61–69.

Berlo, K., S. Tuner, J. Blundy, S. Black, and C. Hawkesworth (2006), Tracing preeruptive magma degassing using (^{210}Pb/^{226}Ra) disequilibria in the volcanic deposits of the 1980–1986 eruption of Mount St. Helens, *Earth Planet. Sci. Lett.*, *249*, 337–349.

Blundy, J., and B. Wood (2003a), Mineral-melt partitioning of uranium, thorium and their daughters, in *Reviews in Mineralogy and Geochemistry*, *Uranium Ser. Geochem.*, vol. 52, edited by B. Bourdon, C. C. Lundstrom, and S. P. Turner, pp. 59–123, Mineral. Soc. of Am., Chantilly, Va.

Blundy, J., and B. Wood (2003b), Partitioning of trace elements between crystals and melts, *Earth Planet. Sci. Lett.*, *210*, 383–397.

Bourdon, B., and K. W. W. Sims (2003), U-series constraints on intraplate magmatism, in *Reviews in Mineralogy and Geochemistry*, *Uranium Ser. Geochem.*, vol.52, edited by B. Bourdon, C. C. Lundstrom, and S. P. Turner, pp. 215–253, Mineral. Soc. of Am., Chantilly, Va.

Bourdon, B., C. H. Langmuir, and A. Zindler (1996a), Ridge-hotspot interaction along the Mid-Atlantic Ridge between 37-30′ and 40-30′N: the U-Th disequilibrium Evidence, *Earth Planet. Sci. Lett.*, *142*, 175–189.

Bourdon, B., A. Zindler, T. Elliott, and C. Langmuir (1996b), Constraints on mantle melting at mid-ocean ridges from global ^{238}U-^{230}Th disequilibrium data, *Nature*, *384*, 231–235.

Bourdon, B., J. L. Joron, C. Claude-Ivanaj, and C. J. Allegre (1998), U-Th-Pa-Ra systematics for the Grande Comore vlocanics: melting progresses in an upwelling plume, *Earth Planet. Sci. Lett.*, *164*, 119–133.

Bourdon, B., S. J. Goldstein, D. Bourles, M. T. Murrell, and C. T. Langmuir (2000), Evidence from ^{10}Be and U series disequilibria on the possible contamination of mid-ocean ridge basalt glasses by sedimentary material, *Geochem. Geophys. Geosyst.*, *1*(8), doi:10.1029/2000GC000047.

Bourdon, B., N. M. Ribe, A. Stracke, A. E. Saal, and S. P. Turner (2006), Insights into the dynamics of mantle plumes from uranium-series disequilibria, *Nature*, *444*, 713–717.

Chabaux, F., D. B. Othman, and J. L. Birck (1994), A new Ra-Ba chromatographic separation and its application to Ra mass-spectrometric measurement in volcanic rocks, *Chem. Geol.*, *114*, 191–197.

Cheng, H., R. L. Edwards, J. Hoff, C. D. Gallup, D. A. Richards, and Y. Asmerom (2000), The half-lives of uranium-234 and thorium-230, *Chem. Geol.*, *169*, 17–33.

Choi, M. S., R. Francois, K. W. W. Sims, M. P. Bacon, S. Legger-Brown, A. P. Fleer, L. A. Ball, D. Schneider, and S. Pichat (2001), Rapid determination of ^{230}Th and ^{231}Pa in seawater by inductively coupled plasma mass spectrometry, *Mar. Chem.*, *76*, 99–112.

Claude-Ivanaj, C., B. Bourdon, and C. J. Allegre (1998), Ra-Th-Sr isotope systematics in Grande Comore Island: A case study of plume-lithosphere interaction, *Earth Planet. Sci. Lett.*, *164*, 99–117.

Cohen, A. S., and K. O'nion (1993), Melting rates beneath Hawaii: Evidence from uranium series isotopes in recent lavas, *Earth Planet. Sci. Lett.*, *120*, 169–175.

Condomines, M., et al. (1987), Short-lived radioactive disequilibria and magma dynamics in Etna volcano, *Nature*, *325*, 607–609.

Condomines, M., P.-J. Gauthier, and O. Sigmarrsson (2003), Timescales of magma chamber processes and dating of young volcanic rocks, in *Reviews in Mineralogy and Geochemistry*, *Uranium Ser. Geochem.*, vol. 52, edited by B. Bourdon, C. C. Lundstrom, and S. P. Turner, pp. 125–174, Mineral. Soc. of Am., Chantilly, Va.

Cooper, K. M., M. R. Reid, M. S. Murrell, and D. A. Clague (2001), Crystal and magma residence at Kilauea Volcano, Hawaii: ^{230}Th-^{226}Ra dating of the 1955 east rift eruption, *Earth Planet. Sci. Lett.*, *184*, 703–718.

Cooper, K. M., S. Goldstein, K. W. W. Sims, and M. S. Murrell (2003), Uranium-series chronology of Gorda Ridge volcanism: New evidence from the 1996 eruption, *Earth Planet. Sci. Lett.*, *206*, 459–475.

DePaolo, D. J. (1988), *Neodymium Isotope Geochemistry: An Introduction*, 187 pp., Springer, Berlin.

Elliott, T. (1997), Fractionation of U and Th during mantle melting: a reprise, *Chem. Geol.*, *139*, 165–183.

Faul, U. (2001), Melt retention and segregation beneath mid-ocean ridges, *Nature*, *410*, 920–923.

Fleer, A. P., and M. P. Bacon (1991), Notes on some techniques of marine particle analysis used at WHOI, in *Marine Particles: Analysis and Characterization*, *Geophys. Monogr. Ser.*, vol. 63, edited by D. C. Hurd and D. W. Spencer, pp. 223–226, AGU, Washington, D. C.

Gauthier, P.-M., and M. Condomines (1999), Pb-Ra radioactive disequilibria in recent lavas and radon degassing; inferences on the magma chamber dynamics at Stromboli and Merapi volcanoes, *Earth Planet. Sci. Lett.*, *172*, 111–126.

Gill, J. B., R. Williams, and K. Bruland (1985), Eruption of basalt and andesite lava degasses ^{222}Rn and ^{210}Po, *Geophys. Res. Lett.*, *12*, 17–20.

Goldstein, S. J., M. T. Murrell, and D. R. Janecky (1989), Th and U isotopic systematics of basalts from the Juan de Fuca and Gorda Ridges by mass spectrometry, *Earth Planet. Sci. Lett.*, *96*, 134–146.

Goldstein, S. J., M. T. Murrell, and R. W. Williams (1993), ^{231}Pa and ^{230}Th chronology of mid-ocean ridge basalts, *Earth Planet. Sci. Lett.*, *115*, 151–159.

Hart, S. R. (1984), A large-scale isotope anomaly in the Southern Hemisphere mantle, *Nature*, *309*, 753–757.

Hart, S. R., and G. A. Gaetani (2006), Mantle Pb Paradoxes: The sulfide solution, *Contrib. Mineral. Petrol.*, *152*, 295–308.

Hart, S. R., et al. (2000), Vailulu'u undersea volcano: The New Samoa, *Geochem. Geophys. Geosyst.*, *1*(12), doi:10.1029/2000GC000108.

Hart, S. R., M. Coetzee, R. K. Workman, J. Blusztajn, K. T. M. Johnson, J. M. Sinton, B. Steinberge, and J. W. Hawkins (2004), Genesis of the western Samoa seamount province: Age, geochemical fingerprint and tectonics, *Earth Planet. Sci. Lett.*, *227*, 37–56.

Hauri, E. H., and S. R. Hart (1993), Re-Os isotope systematics of HIMU and EMII oceanic island basalts from the South Pacific Ocean, *Earth Planet. Sci. Lett.*, *114*, 353–371.

Hauri, E. H., J. A. Whitehead, and S. R. Hart (1994), The nature of entrainment in mantle plumes: A boundary layer model including the effects of temperature and stress-dependent rheologies and depth-dependent physical properties, *J. Geophys. Res.*, *99*, 24,275–24,300.

Heusser, G. (1995), *Annu. Rev. Nucl. Sci.*, *45*, 543–590.

Hirschmann, M. M., and E. M. Stolper (1996), A possible role for pyroxenite in the origin of the garnet signature in MORB, *Contrib. Mineral. Petrol.*, *124*, 185–208.

Holden, N. E. (1990), Total half-lives for selected nuclides, *Pure Appl. Chem.*, *62*, 941–958.

Iwamori, H. (1994), ^{238}U-^{230}Th-^{226}Ra and ^{235}U-^{231}Pa disequilibria produced by mantle melting with porous and channel flows, *Earth Planet. Sci. Lett.*, *125*, 1–16.

Jaffey, A. H., K. F. Flynn, L. E. Glendenin, W. C. Bentley, and A. M. Essling (1971), Precision measurement of half-lives and specific activities of ^{235}U and ^{238}U, *Phys. Rev. C*, *4*, 1889–1906.

Jull, M., P. Kelemen, and K. W. W. Sims (2002), Melt migration and uranium series disequilibria: the combined effect of porous and conduit flow, *Geochim. Cosmochim. Acta*, *66*(23), 4133–4148.

Kokfelt, T. F., K. Hoernle, and F. Hauff (2003), Upwelling and melting of the Iceland plume from radial variation of ^{238}U-^{230}Th disequilibria in postglacial volcanic rocks, *Earth Planet. Sci. Lett.*, *214*, 167.

Ku, T.-L., K. G. Knauss, and G. G. Mathieu (1977), Uranium in open ocean: concentration and isotopic composition, *Deep Sea Res.*, 1005–1017.

Lambert, G., et al. (1985), Volcanic emissions of radionuclides and magma dynamics, *Earth Planet. Sci. Lett.*, *76*, 185–192.

Landwehr, D., J. Blundy, E. Chamorro-Perez, E. Hill, and B. Wood (2001), U-series disequilibria generated by partial melting of spinel lherzolite, *Earth Planet. Sci. Lett.*, *188*, 329–348.

La Tourrette, T. Z., and D. S. Burnett (1992), Experimental determination of U and Th during partitioning between clinopyroxene and natural and synthetic basalt liquid, *Earth Planet. Sci. Lett.*, *110*, 157–159.

La Tourrette, T. Z., A. K. Kennedy, and G. J. Wasserburg (1993), U-Th fractionation by garnet-evidence for a deep source and rapid rise by oceanic basalts, *Science*, *261*, 739–742.

Layne, G. D., and K. W. W. Sims (2000), Analysis of ^{232}Th/^{230}Th in volcanic rocks by Secondary Ionization Mass Spectrometry, *Int. J. Mass Spectrom.*, *203*, 187–198.

Le Roux, L. J., and L. E. Glendenin (1963), Half-life of ^{232}Th, *Proc. Natl. Meet. Nucl. Energy*, 83.

Lundstrom, C. (2000), Models of U-series disequilibria generation in MORB: the effects of two scales of melt porosity, *Phys. Earth Planet. Inter.*, *121*, 189–204.

Lundstrom, C. C., et al. (1994), Compositional controls on the partitioning of U, Th, Ba, Pb, Sr, and Zr between clinopyroxene and haplobasaltic melts: implications for uranium series disequilibria in basalts, *Earth Planet. Sci. Lett.*, *128*, 407–423.

Lundstrom, C., J. Gill, Q. Williams, and M. R. Perfit (1995), Mantle melting and basalt extraction by equilibrium porous flow, *Science*, *270*, 1958–1961.

Lundstrom, C. C., J. Gill, Q. Williams, and B. B. Hanan (1998), Investigating solid mantle upwelling beneath mid-ocean ridges using U-series disequilibria. II. A local study at 33(S mid-Atlantic Ridge, *Earth Planet. Sci. Lett.*, *157*, 167–181.

Lundstrom, C. C., D. E. Sampson, M. R. Perfit, J. Gill, and Q. Williams (1999), Insight into mid-ocean ridge basalt petrogenesis: U-series disequilibria from the Siqueiros Transform, Lamont Seamounts, and East Pacific Rise, *J. Geophys. Res.*, *104*, 13,035–13,048.

Lundstrom, C. C., K. Hoernle, and J. Gill (2003), U-series disequilibria in volcanic rocks from the Canary Islands: Plume versus lithospheric melting, *Geochim. Cosmochim. Acta*, *67*, 4153–4177.

Macdonald, G. A., and T. Katsura (1964), Chemical composition of Hawaiian lavas, *J. Petrol.*, *5*, 82–133.

McDonough, W. F., and S.-S. Sun (1995), The composition of the Earth, *Chem. Geol.*, *120*, 223–253.

McKay, G. A. (1989), Partitioning of REE between major silicate minerals and basaltic melts, in *Geochemistry and Mineralogy of Rare Earth Elements*, vol. 21, *Rev. Mineral.*, edited by B. R. M. Lipin and G. A. McKay, pp. 45–75, Mineral. Soc. of Am., Chantilly, Va.

McKenzie, D. (1985), ^{230}Th-^{238}U disequilibrium and the melting processes beneath ridge axes, *Earth Planet. Sci. Lett.*, *72*, 149–157.

McKenzie, D., and M. J. Bickle (1988), The volume and composition of melt generated by extension of the lithosphere, *J. Petrol.*, *29*, 625–679.

Peate, D. W., C. J. Hawkesworth, P. W. van Calsteren, R. N. Taylor, and B. J. Murton (2001), ^{238}U-^{230}Th constraints on mantle upwelling and plume-ridge interaction along the Reykjanes Ridge, *Earth Planet. Sci. Lett.*, *187*, 259–272.

Pichat, S., K. W. W. Sims, R. François, J. F. McManus, S. Brown-Legger, and F. Albarède (2004), Lower export production during glacial periods in the equatorial Pacific as derived from (^{231}Pa/^{230}Th) measurements in deep-sea sediments, *Paleoceanography*, *19*, PA4023, doi:10.1029/2003PA000994.

Pickett, D. A., and M. T. Murrell (1997), Observations of ^{231}Pa/^{235}U disequilibrium in volcanic rocks, *Earth Planet. Sci. Lett.*, *148*, 259–271.

Pietruszka, A. J., K. H. Rubin, and M. O. Garcia (2001), ^{226}Ra-^{230}Th-^{238}U disequilibria of historic Kilauea lavas (1790–1982) and the dynamics of mantle melting within the Hawaiian plume, *Earth Planet. Sci. Lett.*, *186*, 15–31.

Qin, Z. (1992), Disequilibrium partial melting model and its implications for trace element fractionations during mantle melting, *Earth Planet. Sci. Lett.*, *112*, 75–90.

Reagan, M. K., A. M. Volpe and K. V. Cashman (1992), ^{238}U- and ^{232}Th- series chronology of phonolite fractionation at mount Erebus, Antarctica, *Geochim. Cosmochim. Acta*, *56*, 1401–1407.

Reagan, M. T., F. J. Tepley III, J. B. Gill, M. Wortel, and B. Hartman (2005), Rapid time scales of basalt to andesite differentiation at Anatahan volcano, Mariana Islands, *J. Volcanol. Geotherm. Res.*, *146*, 171–183.

Reagan, M. K., F. J. Tepley III, J. B. Gill, M. Wortel, and J. Garrison (2006), Timescales of degassing and crystallization implied by ^{210}Po-^{210}Pb-^{226}Ra disequilibria for andesitic lavas erupted from Arenal volcano, *J. Volcanol. Geotherm. Res.*, *157*, 135–146.

Reagan, M. K., K. M. Cooper, J. S. Pallister, C. R. Thornber, and M. Wortel (2008), Timing of degassing and plagioclase growth in lavas erupted from Mount St. Helens, 2004–2005, from ^{210}Po–^{210}Pb–^{226}Ra disequilibria, in *A Volcano Rekindled: The First Year of Renewed Eruption at Mount St. Helens, 2004–2006,* edited by D. R. Sherrod, W. E. Scott, and P. H. Stauffer, *U.S. Geol. Surv. Prof. Pap.*, in press.

Ribe, N. M. (1996), The dynamics of plume-ridge interaction 2. Off-ridge plumes, *J. Geophys. Res.*, *101*, 16,195–16,204.

Ribe, N. M., and U. R. Christensen (1999), The dynamical origin of Hawaiian volcanism, *Earth Planet. Sci. Lett.*, *171*, 517–531.

Richardson, C., and D. McKenzie (1994), Radioactive disequilibria from 2D models of melt generation by plumes and ridges, *Earth Planet. Sci. Lett.*, *128*, 425–437.

Robert, J., C. F. Miranda, and R. Muxart (1969), Mesure de la periode du protctinium-231 par microcalorimetrie, *Radiochim. Acta*, *11*, 104–108.

Rubin, K. H. (1997), Degassing of metals and metaloids from erupting seamount and mid-ocean ridge volcanoes: observations and predictions, *Geochim. Cosmochim. Acta*, *61*, 3525–3542.

Rubin, K. H., and J. D. Macdougall (1989), Submarine magma degassing and explosive magmatism at Macdonald (Tamarii) Seamount, *Nature*, *341*, 50–52.

Rubin, K. H., J. D. MacDougall, and M. R. Perfit (1994), ^{210}Po-^{210}Pb dating of recent volcanic eruptions on the sea floor, *Nature*, *368*, 841–844.

Rubin, K. H., M. C. Smith, and E. C. Bergmanis (2005), Minimum speed limit for ocean ridge magmatism from ^{210}Pb–^{226}Ra–^{230}Th disequilibria, *Nature*, *437*, 22.

Saal, A. E., and J. A. Van Orman (2004), The ^{226}Ra enrichment in oceanic basalts: Evidence for melt-cumulate diffusive interaction processes within the oceanic lithosphere, *Geochem. Geophys. Geosyst.*, *5*, Q02008, doi:10.1029/2003GC000620.

Salters, V. J. M. (1996), The generation of mid-ocean ridge basalts from the Hf and Nd perspective, *Earth Planet. Sci. Lett.*, *141*, 109–123.

Salters, V. J. M., and S. R. Hart (1989), The hafnium paradox and the role of garnet in the source of mid-ocean ridge basalts, *Nature*, *342*, 420–422.

Salters, V. J. M., and J. E. Longhi (1999), Trace element partitioning during the initial stages of melting beneath mid-ocean ridges, *Earth Planet. Sci. Lett.*, *166*, 15–30.

Salters, V. J. M., J. E. Longhi, and M. Bizimis (2002), Near solidus trace element partitioning at pressures up to 3.4 GPa, *Geochem. Geophys. Geosyst.*, *3*(7), 1038, doi:10.1029/2001GC000148.

Sato, J. (2003), Natural radionuclides in volcanic activity, *Appl. Radiat. Isotopes*, *58*, 393–399.

Sato, K., and J. Sato (1977), Estimation of gas releasing efficiency from ^{226}Ra-^{222}Rn disequilibrium, *Nature*, *266*, 439–440.

Shaw, D. M. (1970), Trace element fractionation during anatexis, *Geochim. Cosmochim. Acta*, *34*, 237–243.

Sigmarsson, O., S. Carn, and J. C. Carracedo (1998), Systematics of U-series nuclides in primitive lavas from the 1730-36 eruption in Lanzarote, Canary Islands, and the implications for the role of garnet pyroxenite during oceanic basalt formation, *Earth Planet. Sci. Lett.*, *162*, 1337–1351.

Sims, K. W. W., and D. J. DePaolo (1997), Inferences about mantle magma sources from incompatible element concentration ratios in oceanic basalts, *Geochim. Cosmochim. Acta*, *61*, 765–784.

Sims, K. W. W., and P.-J. Gauthier (2007), From source to surface: U-series constraints on the processes and timescales of magma generation, evolution and degassing, paper presented at International Conference on Evolution, Transfer and Releases of Magmas and Volcanic Gases, Acad. Sin., Taipei.

Sims, K. W. W., and S. R. Hart (2006), Comparison of Th, Sr, Nd and Pb isotopes in oceanic basalts: Implications for mantle heterogeneity and magma genesis, *Earth Planet. Sci. Lett.*, *245*, 743–761.

Sims, K. W., D. J. DePaolo, M. T. Murell, W. S. Baldridge, S. J. Goldstein, and D. A. Clague (1995), Mechanisms of magma generation beneath Hawaii and mid-ocean ridges: Uranium/Thorium and Samarium/Neodymium isotopic evidence, *Science*, *267*, 508–512.

Sims, K. W. W., D. J. DePaolo, M. T. Murell, W. S. Baldridge, S. Goldstein, D. A. Clague, and M. Jull (1999), Porosity of the melting zone and variations in solid mantle upwelling rate beneath Hawaii: Inferences from ^{238}U-^{230}Th-226Ra and ^{235}U-^{231}Pa disequilibria, *Geochim. Cosmochim. Acta*, *63*, 4119–4138.

Sims, K. W., N. Mattielli, T. Elliott, P. Kelemen, D. J. DePaolo, D. F. Mertz, C. Devey, and M. T. Murrell (2001), ^{238}U and ^{230}Th excesses in Kolbeinsey ridge basalts, *Eos Trans. AGU*, *82*(47), Fall Meet. Suppl., Abstract V12A-0952.

Sims, K. W. W., et al. (2002), Chemical and isotopic constraints on the generation and transport of magma beneath the East Pacific Rise, *Geochim. Cosmochim. Acta*, *66*, 3481–3504.

Sims, K. W. W., et al. (2008), An inter-laboratory assessment of the thorium isotopic composition of synthetic and rock reference materials, *Geostand. Geoanal. Res.*, *32*(1), 65–91.

Sleep, N. H. (1990), Hot spots and mantle plumes: some phenomenology, *J. Geophys. Res.*, *95*, 6715–6736.

Spiegelman, M., and T. Elliot (1993), Consequences of melt transport for U-series disequilibrium in young lavas, *Earth Planet. Sci. Lett.*, *118*, 1–20.

Staudigel, H., S. R. Hart, A. A. P. Koppers, C. Constable, R. Workman, M. Kurz, and E. T. Baker (2004), Hydrothermal venting at Vailulu'u Seamount: The smoking end of the Samoan chain, *Geochem. Geophys. Geosyst.*, *5*, Q02003, doi:10.1029/2003GC000626.

Staudigel, H., et al. (2006), Vailulu'u Seamount, Samoa: Life and death on an active submarine volcano, *Proc. Natl. Acad. Sci.*, *103*, 6448–6453.

Stracke, A., V. J. M. Salters, and K. W. W. Sims (1999), Assessing the presence of pyroxenite in the source of Hawaiian basalts: Hafnium-neodymium-thorium isotope evidence, *Geochem. Geophys. Geosyst.*, *1*(1), doi:10.1029/1999GC000013.

Stracke, A., A. Zindler, V. J. M. Salters, D. McKenzie, and K. Grönvold (2003), The dynamics of melting beneath Theistareykir, northern Iceland, *Geochem. Geophys. Geosyst.*, *4*(10), 8513, doi:10.1029/2002GC000347.

Sturm, M. E., S. J. Goldstein, E. M. Klein, J. A. Karson, and M. T. Murrell (2000), Uranium-series age constraints on lavas from the axial valley of the Mid-Atlantic Ridge MARK area, *Earth Planet. Sci. Lett.*, *181*, 61–70.

Tepley, F. J. I., C. C. Lundstrom, K. W. W. Sims, and R. Hekinian (2004), U-series disequilibria in MORB from the Garrett Transform and implications for mantle melting, *Earth Planet. Sci. Lett.*, *223*, 79–97.

Thomas, L. E., C. J. Hawkesworth, P. Van Calsteren, S. P. Turner, and N. W. Rodgers (1999), Melt generation beneath ocean island: A U-Th-Ra isotope study from Lanzarote in the Canary Islands, *Geochim. Cosmochim. Acta*, *63*, 4081–4099.

Thurber, D. (1962), Anomalous $^{234}U/^{238}U$ in nature, *J. Geophys. Res.*, *67*, 4518.

Tuli, J. K. (2000), Nuclear wallet cards, 114 pp., Brookhaven Natl. Lab., Upton, N. Y.

Turner, S., C. Hawkesworth, N. Rodgers, and P. King (1997), U-Th disequilibria and ocean island basalt generation in the Azores, *Chem. Geol.*, *139*, 145–164.

Turner, S. P., S. Black, and K. Berlo (2004), ^{210}Pb-^{226}Ra and ^{226}Ra-^{230}Th systematics in young arc lavas: Implications for magma degassing and ascent rates, *Earth Planet. Sci. Lett.*, *227*, 1–16.

Watson, S., and D. McKenzie (1991), Melt generation by plumes: a study of Hawaiian volcanism, *J. Petrol.*, *32*, 501–537.

Widom, E., R. W. Carlson, J. B. Gill, and H. U. Schmincke (1997), Th-Sr-Nd-Pb isotope and trace element evidence for the origin of the Sao Miguel, Azores, enriched mantle source, *Chem. Geol.*, *140*, 49–68.

Williams, R. W., and J. B. Gill (1989), Effects of partial melting on the uranium decay series, *Geochim. Cosmochim. Acta*, *53*, 1607–1619.

Workman, R. K., and S. R. Hart (2005), Major and trace element composition of the depleted MORB mantle (DMM), *Earth Planet. Sci. Lett.*, *231*, 53–72.

Workman, R. K., S. R. Hart, M. Jackson, M. Regelous, K. A. Farley, J. Blusztajn, M. Kurz, and H. Staudigel (2004), Recycled metasomatized lithosphere as the origin of the Enriched Mantle II (EM2) end-member: Evidence from the Samoan Volcanic Chain, *Geochem. Geophys. Geosyst.*, *5*, Q04008, doi:10.1029/2003GC000623.

Workman, R. K., E. Hauri, S. R. Hart, J. Wang, and J. Blusztajn (2006), Volatile and trace elements in basaltic glasses from Samoa: Implications for water distribution in the mantle, *Earth Planet. Sci. Lett.*, *241*, 932–951.

Zindler, A., and S. R. Hart (1986), Chemical geodynamics, *Ann. Rev. Earth Planet. Sci.*, *14*, 493–571.